Scientific Report 2009

Institute for Energy Research-
Safety Research and Reactor Technology (IEF-6)

Safety Research for Nuclear Waste Disposal

Content **page**

MC simulation of thermal neutron flux of large samples irradiated by 14 MeV neutrons

Y. Bai[1], D. Wang[1], E. Mauerhofer[2], J. Kettler[2]

[1]*School of Nuclear Science and Engineering, Shanghai Jiao Tong University, 200240 Shanghai, China*
[2]*Institut für Energieforschung – Sicherheitsforschung und Reaktortechnik (IEF-6), Forschungszentrum Jülich*
Corresponding author: e.mauerhofer@fz-juelich.de

Abstract: The response of a 14 MeV neutron-based prompt gamma neutron activation analysis (PGNAA) system, i.e. the prompt gamma-rays count rate and the average thermal neutron flux, is studied with a large concrete sample and with a homogeneous large sample, which is made of polyethylene and metal with various concentrations of hydrogen and cadmium using the MCNP-5 (Monte Carlo N-Particle) code. The average thermal neutron flux is determined by the analysis of the prompt gamma-rays using the thermal neutron activation of hydrogen in the sample, and the thermal and fast neutron activation of carbon graphite irradiation chamber of the PGNAA-system. Our results demonstrated that the graphite irradiation chamber of the PGNAA-system fairly operates, and is useful to estimate the average thermal neutron flux of large samples with various compositions irradiated by 14 MeV neutrons.

Introduction

In Germany, the declaration and balancing of toxic substances in low and intermediate level radioactive waste (LILW) have become obligatory as a result of the plan-approval for disposal Konrad [1]. Depending on its origin, LILW may contain toxic elements (Pb, Cd, Hg, and alkali metals), anions (nitrates, sulphates, chlorides, and chlorates), and toxic organic chemical compounds [2]. Radioactive waste containing such toxic substances must comply with the regulations defined by the German authority and their properties need to be taken into account for a safe disposal.

In order to achieve this, the limiting values for toxic elements and substances were defined by the Federal Office of Radiation Protection (BfS)[3] for the final disposal of radioactive waste packages in the mine Konrad. To determine toxic elements in radioactive waste packages, a non-destructive analytical technique based on PGNAA (Prompt- Gamma-Neutron-Activation-Analysis) with a 14 MeV neutron generator is in development at the Institute of Energy Research-Safety Research and Reactor Technology, Forschungszentrum Jülich, Germany. In the first step, a PGNAA-system consisting of a 14 MeV neutron generator for sample irradiation, an HPGe detector for prompt-gamma ray measurement, and a graphite irradiation chamber was designed for the investigation of large samples with a maximal volume of 50 L.

In this paper, the prompt γ-ray count rate and the average thermal neutron flux in the sample for the PGNAA-system was studied with a large concrete sample and with a homogeneous large sample made of polyethylene (PE) and metal with various H and Cd contents using the MCNP-5 code. To determine the average thermal neutron flux in large samples of various compositions, a new method was proposed using the prompt-gamma rays at 2.22 MeV produced by thermal neutron activation of hydrogen in the sample, and at 4.44 MeV and 4.95 MeV produced by fast and thermal neutron activation of carbon in the graphite chamber and in the sample, respectively.

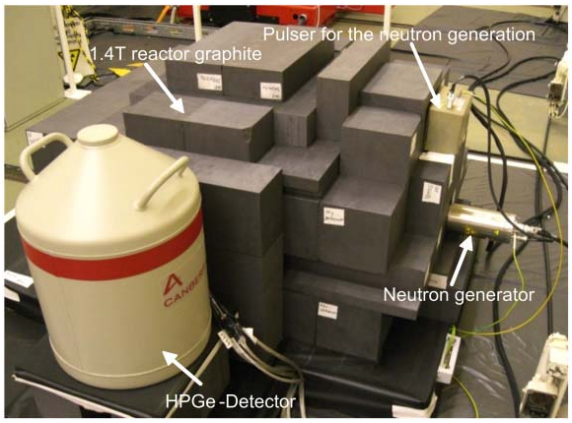

Fig. 1: Side views of the PGNAA-system in the experimental hall with the HPGe-detector in front, the neutron generator on the right side and the graphite irradiation chamber.

MCNP5 modeling

The PGNAA-system was modeled according to the experimental setup (Fig. 1). The investigated drum was placed in an irradiation chamber made exclusively of graphite as neutron moderator and reflector. Out of radioprotection purpose, the chamber wall was about 40 cm thick, and the inner volume was 40 cm × 40 cm × 50 cm. Hydrogenous materials like PE or paraffin were prohibited in the irradiation chamber, so as to determine hydrogen content of the drum matrix using the 2.22 MeV γ-ray. The drum was irradiated with 14 MeV neutrons from a D-T neutron generator (GENIE 16GT, EADS SODERN). The deuterium beams irradiate the tritium target located at mid-height of the drum, and a 35-cm distance was kept from its centre. The prompt γ-rays was detected with a 104% n-type HPGe detector (Canberra). The detector was surrounded by ^{6}LiF plates to avoid thermal neutron capture in the Ge crystal. The distance between the detector window and the drum centre was 35 cm so that a 50 L drum was fully analyzed.

In the MCNP model, the 14 MeV neutron source was defined as a disc source emitting 10^8 n·s^{-1}(4π), and the HPGe detector was described as a 8×8 cylinder of natural germanium. To be like with a real HPGe detector, track lengths of the γ-rays were simulated using the so called "pulse height tally" and the Gaussian Energy Broadening function (GEB), which is related to energy resolution of the physical detector. The 50 L steel drum with 1.5 mm wall was filled with dry concrete or a mixture of PE and metal.

Contents of the dry concrete were: O, 51.6%; Si, 37%; Ca, 8.9%; Al, 0.85%; K, 0.7%; Mg, 0.57%; Fe, 0.45%; H, 0.41%; Mn, 0.0294%; and Cl, 0.0097%. It was about 115 kg, with a density of 2.35 g·cm^{-3}. In order to simulate the samples with higher H content, the silicon content was replaced by hydrogen. Composition of the PE and metal mixture was: O, 24.7 α%; Na, 5.9 α%; Al, 11.8 α%; Si, 28.2 α%; Ca, 11.8 α%; Fe, 11.8 α%; and Cu, 5.9 α%, where α = (1–C_{PE} /100) and C_{PE} is the PE content. For polyethylene, the carbon content changes with hydrogen content at a mass ratio of 6/1. And the mixture of PE and metal was 115 kg, with an average density of 2.3 g·cm^{-3}.

In the simulations, Cd content of the samples increased from 0 to 1000 ppm, and hydrogen content from 0 to 4%. Each simulation calculated 10^9 particles, for a high statistical precision in terms of relative error and variance of variance (vov), within an accuracy interval of 0.2% (1σ).

Prompt gamma ray count rates

As an example, the prompt gamma spectrum (Fig. 2) was obtained by MCNP5 with the concrete sample of 500-ppm cadmium. A large number of prompt γ-rays were observed from the fast and thermal neutron activation of the sample, the graphite chamber and the steel drum. The prompt γ-rays at 2.22 MeV produced by thermal neutron activation of hydrogen in the sample, and at 4.44 MeV and 4.95 MeV produced by fast and thermal neutron activation of carbon in the graphite chamber and in the sample were labeled. They were used to monitor the average thermal neutron flux of the samples. The major prompt γ-ray of Cd at 0.558 MeV was also marked in the figure.

The count rate at 2.22 MeV with the H and Cd in the two samples is shown in Fig. 3. Under given Cd concentration, the count rate at 2.22 MeV increases with the H concentration, which acted as fast neutron moderator, hence an increase of the average thermal neutron flux. The concrete sample had higher counts than the PE and metal mixture, reflecting a difference in the absorption of thermal neutrons. Given the H concentration, the count rate at 2.22 MeV decreased with the Cd concentration due to the absorption of its thermal neutrons. This was more remarkable in the concrete sample than in the mixture of PE and metal because of the composition difference, and the higher the Cd concentration, and the lower the difference for the two samples. Thus, the count rate at 2.22 MeV may be used to monitor the average thermal neutron flux in a specific sample.

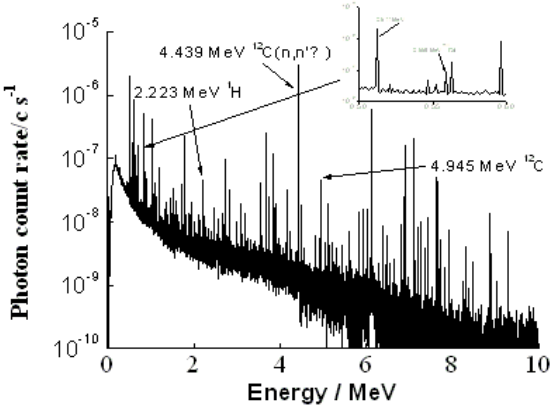

Fig. 2: Simulated prompt gamma spectrum of concrete sample (115 kg) of 500 ppm cadmium. The simulation was performed by MCNP5, with 10^8 n·s^{-1} of 14 MeV neutrons, which was normalized to 1.

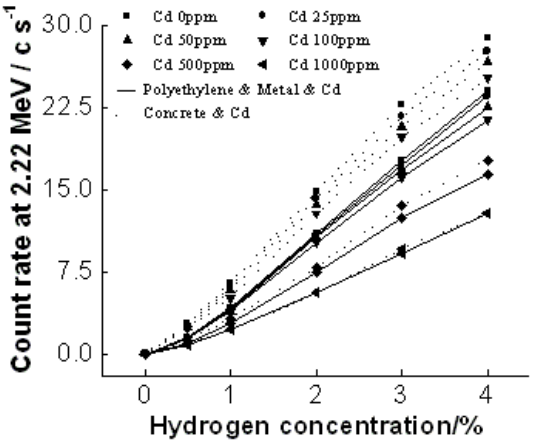

Fig. 3: Count rate of the prompt γ-ray at 2.22 MeV calculated by MCNP5 with thermal neutron activation of H in the sample, as function of the H and Cd concentration in the two materials.

The dependence of the count rate at 4.44 MeV on the H and Cd contents in the two samples is shown in Fig. 4. The value, which was independent of the Cd content, i.e. the thermal neutron absorption, only depends on moderation properties of the sample, and decreased linearly with the H concentration. In the mixture of the samples, however, a break of the linearity was observed due to containing 3% to 4% hydrogen except for a large amount of polyethylene. Given the H concentration, the count rate was lower in the concrete sample than in the mixed samples, as the former is a better absorber of fast neutrons than the latter. The macroscopic neutron cross section of 14 MeV neutrons was 0.115 cm^{-1} for the concrete sample, and was 0.0827 cm^{-1} for the mixture without polyethylene, and that was 0.0964 cm^{-1} for the mixture of 24% PE (4% H). Thus the count rate at 4.44 MeV may be used to monitor the moderation and absorption of fast neutrons in the sample.

The count rate at 4.95 MeV varied with the H and Cd contents in the two samples (Fig. 5). The behavior was much more complex than at 2.22 MeV and 4.44 MeV. Given the Cd concentration, the count rate increased for a lower than 1% hydrogen, and reached a constant for hydrogen concentrations of 1% to 2% in the concrete sample, and for that of 1% to 3% in the PE and metal mixture. At the highest H concentrations, the count rate decreased in the concrete sample due to its thermal neutron absorption, and increased in the mixed samples due to the large amount of the carbon. Given the H concentration, the count rate at 4.95 MeV decreased with increasing Cd concentrations due to its thermal neutron absorption, which reflected the moderation of fast neutrons and the absorption of thermal neutrons in the sample.

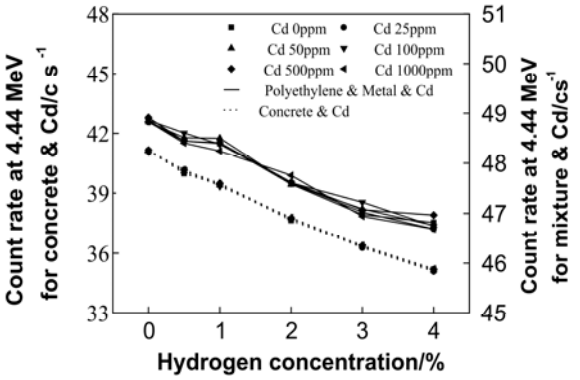

Fig. 4: Count rate of the prompt γ-ray at 4.44 MeV calculated by MCNP5 with fast neutron activation of carbon (graphite cell), as a function of the H and Cd contents in the two materials.

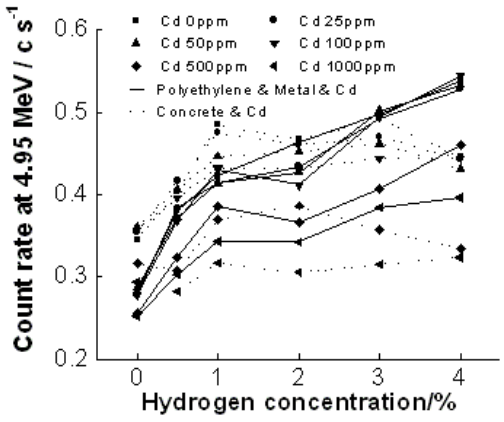

Fig. 5: Count rate of the prompt γ-ray at 4.95 MeV calculated by MCNP5 with thermal neutron activation of carbon (graphite cell) as a function of the H and Cd contents in the two materials.

The count rate at 0.558 MeV depended on the H and Cd concentration in the two samples (Fig. 6). Given the Cd concentration, the rate increased non-linearly for a lower than 2 % hydrogen in the concrete sample, and lower than 3% hydrogen in the mixed samples. For high hydrogen and lower cadmium than 500 ppm, the rate decreased due to the thermal neutron absorption by hydrogen. For higher cadmium than 500 ppm, the rate increased. Given the H content, the rate increased with the Cd concentration and reached a saturation value due to the absorption of thermal neutrons by cadmium.

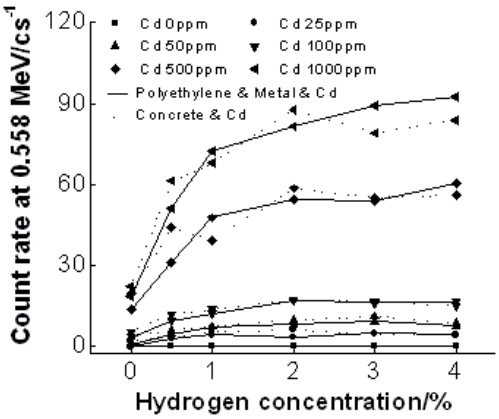

Fig. 6: Count rate of the prompt γ-ray at 0.558 MeV calculated by MCNP5 with thermal neutron activation of cadmium in the sample as a function of the H and Cd concentration in the two materials.

Thermal neutron flux

Figure 7 shows dependence of the average thermal neutron flux on the H and Cd concentration in the two samples. Given the Cd concentration, the average thermal neutron flux increased non-linearly with the H concentration, whereas it decreased non-linearly with increasing Cd concentration under given H content.

In order to find a general analytical expression of the average thermal neutron flux based on the count rates, the average thermal neutron flux, Φ_{th}, was calculated by MCNP5 without cadmium in the two materials, i.e. the strong thermal neutrons absorber was first fitted by function of the prompt γ-ray count rate of hydrogen at 2.22 MeV, Z_H, using Eq. (1),

$$\Phi = \Phi_0 + \Phi_{max} Z_H / (C + Z_H) \quad (1)$$

where, Φ_0 was the average thermal neutron flux without hydrogen, Φ_{max} was its maximum value, and C was sample composition dependent corrective factor taking into account the moderation of the fast neutrons. In the concrete sample, fitting the Φ should lead to Φ_0 = 3138 ± 355 n·cm^{-2}·s^{-1}, Φ_{max} = 15063 ± 488 n·cm^{-2}·s^{-1}, and C = 4.11 ± 0.49 counts·s^{-1} with a regression coefficient of 0.998. In the PE and metal mixture, Φ_0 = 2173 ± 242 n·cm^{-2}·s^{-1}, Φ_{max} = 15352 ± 547 n·cm^{-2}·s^{-1}, and C = 7.44 ± 0.49 counts·s^{-1} with a regression coefficient of 0.999. The Φ_0 values are in good agreement with of that of the MCNP5 calculation (3162 and 2021 n·cm^{-2}·s^{-1}). Taking into account the errors, the two materials have the same Φ_{max} and the averaged Φ_{max} of 15207 ± 204 n·cm^{-2}·s^{-1}) was used for the following calculation.

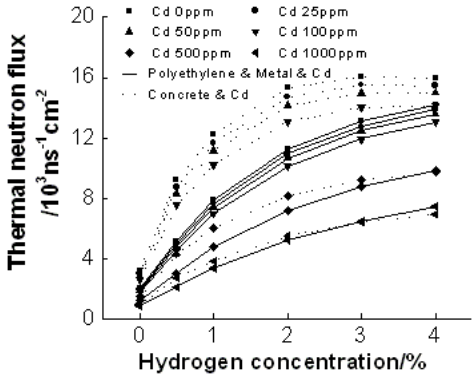

Fig. 7: Average thermal neutron flux calculated by MCNP-5 varied as function of the hydrogen and cadmium concentration for the two materials.

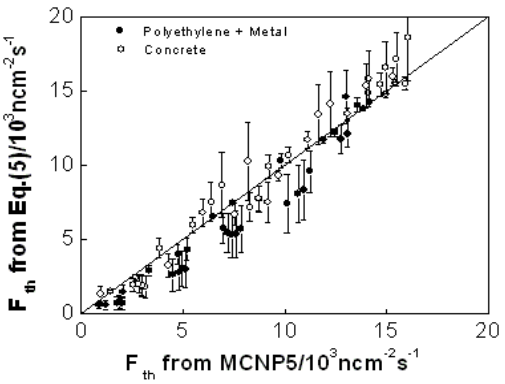

Fig. 8: The comparison of the average thermal neutron flux calculated by mean of Eq. (6) with by MCNP5 for the two materials.

In a next step, a factor taking into account the relative effect of the concrete sample on the moderation of the fast neutrons was defined using the prompt γ-ray count rate at 4.44 MeV, $Z_{C,fast}$, which was produced by the fast neutron activation of carbon as,

$$\alpha = Z_{C,fast}/Z^{ref}_{C,fast} \quad (2)$$

where, $Z^{ref}_{C,fast}$ is the average count rate at 4.44 MeV in the concrete samples without cadmium, to be free from Cd influence on fast neutron moderation (Fig. 4). The count rate at 2.22 MeV, Z_H, can be calculated by:

$$Z^{ref}_{C,fast} = a_0 + a_1 Z_H + a Z_H^2 \quad (3)$$

with a_0 = 41.08 ± 0.06, a_1 = –183.88 ± 8.55 and a_2 = 889.77 ± 41.37 the coefficients of the fit with a regression coefficient of 0.999.

A factor considering the relative influence of the concrete sample on the absorption of the thermal neutron without cadmium was derived from the prompt gamma-ray count rate at 4.95 MeV, $Z_{C,thermal}$, which was produced by the thermal neutron activation of carbon as follows:

$$\beta = Z_{C,thermal}/Z^{ref}_{C,thermal} \quad (4)$$

where, $Z_{C,thermal}$ = 0.453 ± 0.035 counts·s^{-1} is the mean count rate at 4.95 MeV in the cadmium-free concrete samples.

Finally, the average thermal neutron flux, Φ_{th}, can be calculated for any samples with the lower than 4% hydrogen, and with the lower than 1000 ppm cadmium, as well as other elements, which showed a strong absorption of thermal neutron using the following semi empirical formula:

$$\Phi_{th} = \alpha\,\beta^2\,[\alpha^2\Phi_0 + \Phi_{max} Z_H/(\alpha^{5/2}\,C + Z_H)] \quad (5)$$

where, Φ_0 = 3138 ± 355 n·cm^{-2}·s^{-1}, Φ_{max} 15207 ± 204 n·cm^{-2}·s^{-1}, and C = 4.11 ± 0.49 counts·s^{-1}, obtained from the analysis of the average thermal neutron flux without Cd in the concrete sample. The values of Φ_{th} obtained by Eq. (5) were compared with that of the MCNP5 calculation, both were in good agreement within a relative error of 16 % (Fig. 8), and the deviation for the two data sets was –11 ± 23%.

According to the PGNAA system, therefore, Eq.(5) led to a fairly good estimation for the average thermal neutron flux in a homogeneous large sample of 50 L, irradiated by a 14 MeV neutron source emitting the 10^8 n·s^{-1}(4π). Any modification of the PGNAA system and a change of the sample volume should impact on the prompt gamma-ray count rates, and was necessary for a new parameterization.

Conclusion

In this work, the demonstration that the average thermal neutron flux in large samples irradiated by 14 MeV neutrons may be estimated from the prompt gamma-rays produced by the thermal neutron activation of hydrogen in the sample, and by the thermal and fast neutron activation of carbon in the sample and the graphite irradiation chamber has been proved based on the simulation by MCNP-5. The analytical expression to calculate the average thermal neutron flux is specific to the PGNAA-system described in this work i.e. to the amount and thickness of graphite surrounding the sample and to the relative position of the gamma-ray detection system to the 14 MeV neutron source.

References

[1] Niedersächsisches Umweltministerium; Planfeststellungsbeschuss für die Errichtung und den Betrieb des Bergwerkes Konrad in Salzgitter als Anlage zur Endlagerung fester oder verfestigter radioaktiver Abfälle mit vernachlässigbarer Wärmeentwicklung, Bekanntmachung des NMU vom 20.05.2002. Niedersächsisches Ministerialblatt, Hannover, Nds. MBl. Nr. 21/2002, 808.

[2] International Atomic Energy Agency. IAEA-TECDOC- 1325: Management of low and intermediate level radio- active wastes with regard to their chemical toxicity, IAEA, Vienna, December 2002, 3-10.

[3] Bundesamt für Strahlenschutz. Planfeststellungsbeschluss für die Errichtung und den Betrieb des Bergwerkes Konrad in Salzgitter. 2002, 191-196.

Product control of waste products with new coating materials

H. Krumbach[1], H.-J. Steinmetz[1], R. Odoj[1], W. Wartenberg[2], H. Grunau[3]

[1] *Institute for Energy Resarch – Safty Research and Reactor Technology (IEF-6), Forschungszentrum Jülich*
[2] *Company Nuclitec GmbH Braunschweig*
[3] *Company Eisenwerk Bassum m.b.H*
Corresponding author: h.krumbach@fz-juelich.de

Abstract: The previously conditioned radioactive waste has to be suitable for a longer-term interim storage. They have to be treated in a way that they are chemically stable and that their integrity is guaranteed for a long time. That's why the waste product or the container is covered/ coated for special waste such as hygroscopic waste or waste that includes aluminium. The Product Control Group for radioactive waste (PKS) has to proof the suitability of the so-treated waste for the repository KONRAD on behalf of the Federal Office for Radiation Protection (BfS). This has to be done before the delivering. In this context the PKS also assesses the suitability of new coating materials for low radioactive waste products or containers and their correct technical application.

Objectives

By the time radioactive waste has to be conditioned and interim stored according to the final conditions requirements for disposal radioactive waste - „Anforderungen an endzulagernde radioaktive Abfälle – Schachtanlage Konrad“ [1] (Stand: Dezember 1995).
The waste products or waste packages must be chemically stable and technically in perfect condition until the date of the disposal. Regarding different wastes such as ash, concentrates (hygroscopic waste) or waste with aluminium, the integrity of the packaging shall be ensured by a special anti-corrosion coating. Before the application of such a coating their suitability has to be examined by experts and released by the Federal Office for Radiation Protection.
Because there is currently only a technical application for polyurethane coating it is also only part of the assessment by the product inspection for radioactive waste.

In the context of two research projects, the possibilities for the coating or backfill of waste products were inspected.
In this context the Institute of Materials Engineering at the University of Dortmund accomplishes long-term studies of polyurethane (PU) coated samples [2].
The second research project at the Institute for Energy Research 6 (IEF-6) of the Research Center Juelich, deals with the implementation of silicon plastics as coating or filling materials [3].
A major focus of those investigations was to ascertain the suitability of both materials in terms of corrosion-protection.
The using of silicon plastics as coating or backfill is mainly based on theoretical considerations and laboratory tests. These investigations show that silicon plastics can be used for the filling of containers with radioactive waste and are not suitable for the coating of radioactive waste products.

The Product Control Group has to conduct studies in order to assess the suitability of various coating materials. Those investigations proof, whether these new coating materials are in line with the disposal conditions requirements for radioactive waste „Anforderungen an endzulagernde radioaktive Abfälle - Schachtanlage Konrad [1] (Stand: Dezember 1995)”.

Polyurethan coating

The coating with polyurethane is the most developed process in the industrial application.
A polyurethane coating is used as corrosion protection for the walls at the dock "Benser - Siel" in a long time test. There, the materials demonstrated the effectiveness as a corrosion protection for more than 20 years. The investigations by the Department of Materials Technology at the University of Dortmund also assess the suitability as a long-term corrosion protection.
In nuclear technology polyurethane was initially used as corrosion protection for KONRAD containers.
The coating of waste products can be used for corrosion protection as well and on the other hand; the material properties of polyurethane can be used as a further protective effect for the waste products.
The coating with polyurethane avoids the penetration of oxygen in hygroscopic waste other chemical reactions in the waste products can be blocked also. The basic property such as fire behaviour and thermal properties of polyurethane were examined in the approval of the coating material as a coating for disposal containers.
The PKS evaluation covers the technical suitability for coating material for waste products (water permeability, impact strength). Several techniques are used for the application of polyurethane. The common techniques for the coating of KONRAD – containers and barrels are spray proceedings (Fig. 1), while the coating of super compacted waste is made by cast proceedings (Fig. 2).

Fig. 1: Coating with Polyurethane

Fig. 2: Pellet in a cast form

Results

The PKS's own assessments concerning the acceptability for reposition of new coating materials have shown that the polyurethane coating of radioactive waste products is adequate.

Polysiloxane which has been investigated alternatively at the beginning is not suitable as a coating. Because this material is permeable to air it has only got a limited protective function.

The coating of radioactive waste products or containers with polyurethane can be used in cast proceeding as well as spraying procedures. For drums and containers the spray technique turned out to be advantageous. For super compacted waste (pellets) the cast proceeding has got considerable advantages.

The suitability of polyurethane as corrosion protection has been demonstrated by studies at the University of Dortmund and in practice by the coating of a port basin.

For reasons of economy the polyurethane coating is used only for problem waste.

The coating meets the demands of the final repository for radioactive waste “Schachtanlage KONRAD”.

References

[1] Peter Brennecke, Bundesamt für Strahlenschutz, Fachbereich Nukleare Entsorgung und Transport, Salzgitter: „Anforderungen an endzulagernde radioaktive Abfälle“ (Endlagerungsbedingungen, Stand: Dezember 1995) – Schachtanlage Konrad –, Dezember 1995, ET-IB-79

[2] Prof. Dr.-Ing. Friedrich-Wilhelm Bach, Lehrstuhl für Werkstofftechnologie, Fakultät Maschinenbau, Universität Dortmund: „Prüfbericht: Langzeituntersuchungen von PU - beschichteten Proben“, 2000

[3] Prof. Dr. R. Odoj, FZJ, Dr. S. Maischak, FZJ, W. Pfeifer, FZK, L Valencia, FZK, L. Schneider, A. Rohr and C. Herzog, Stoller Ingenieurtechnik: “Application of Polysiloxanes for the Treatment of Radioactive Waste to Guarantee Safe Long Term Storage”, Waste Management 2004 Symposium, Tucson, Arizona 2004

2009 annual report of PKS-WAA

E. Harren, F. Kreutz, S. Maischak, S. Schneider, T. Steinhardt, H. Tietze-Jaensch

Institut für Energieforschung – Sicherheitsforschung und Reaktortechnik (IEF-6), Forschungszentrum Jülich
Corresponding author: h.tietze@fz-juelich.de

Abstract: Throughout 2009 the Product Quality Control Office for Reprocessed Waste (PKS-WAA) fulfilled its regular expert surveillance tasks on radioactive waste residues to be returned from reprocessing plants in France and the UK. In Oct 2009 the German vitrification plant VEK became fully operational, and its vitrified residues are also checked by PKS before loading into a CASTOR flask. Final process qualification of the AREVA NC nuclear measurement station P2 at the supercompaction plant in La Hague is in progress. Accompanying R&D work on γ- and neutron radiation emissions has commenced, and the upcoming process qualification of French MAW glass residues (CSD-B) is being prepared for. PKS takes an active role in national and international expert and consultancy commissions.

In 1985 the Product Quality Control Office for Reprocessed Waste (PKS-WAA) has been installed at the Institute for Energy Research (IEF-6) on request of the German Federal Office for Radiation Protection (BfS). PKS gives advice to BfS on the basis of §20 ATG (German atomic act) as an independent consulting expert group in order to verify the compliance of radioactive waste residue properties with repository relevant acceptance criteria. Thus, the product quality control work contributes significantly to the safety of a nuclear waste repository.

PKS-WAA thoroughly evaluates the scientific and technical justification of the radioactive waste conditioning and residue production processes and methods (so-called production process approval). The vitrification and waste conditioning plants are inspected at least twice a year to assure their performance to comply with the approved process specifications. At the Sellafield site, UK, the process approval comprises the vitrification plant and, by now, the residue export facility for uploading CASTOR flask for their transport to Germany. Whereas in France, no more HLW vitrified waste for Germany is in production while shipment is still in progress. In addition other waste streams are subject of a recent ongoing process approval for the German side, e.g. the nuclear measurement station P2 of the metallic waste compaction plant or the CSD-B waste stream of vitrified medium level effluents, mainly from tank rinsing operations in the spent fuel dissolution plant at La Hague. PKS evaluates the productions processes and reports its recommendations directly to BfS to decide and eventually grant their production approval or denial.

All accompanying documentation and radioactive inventory declaration of each waste container that is to be returned from the reprocessing plants and disposed of in a German long-term repository are thoroughly checked prior to loading and transportation.

The Karlsruhe vitrification plant VEK has become fully operational is Oct. 2009. The first CASTOR flask has been loaded, which means that all production thereto has been conform and compliant with the product specifications and repository relevant regulations.

A team of three scientists, two engineers and a Ph.D student form the group of the Product Quality Control Office for Reprocessed Waste (PKS-WAA).

Dedicated R&D is conducted on numerical Monte Carlo methods and simulation programmes to investigate the gamma- and neutron emission from highly compacted metallic waste residues. Questions like impact of varying concentration / activity and geometrical position of key nuclides in a heterogeneous material embedding are being addressed. The goal is to develop easy-to-use proof tools for examination and evaluation of disposal relevant nuclear properties of radioactive metallic waste compounds.

Individual experts of PKS-WAA participate in national and international advisory councils and consulting expert groups.

Determination of the chemical bond of carbon-14 in neutron-irradiated nuclear graphite

D. Vulpius, W. von Lensa

Institute for Energy Research - Safety Research and Reactor Technology (IEF-6), Forschungszentrum Jülich
Corresponding author: d.vulpius@fz-juelich.de

Abstract: The chemical bond of carbon-14 in neutron-irradiated nuclear graphite was identified by secondary ion mass spectroscopy and Raman spectroscopy. To support our study ion implantation experiments were carried out with carbon-12 and nitrogen-14. The carbon-12 ions should simulate the entry of carbon-14 in graphite, and the nitrogen-14 ions should verify in which chemical form nitrogen is present in graphite after neutron irradiation in a nuclear reactor. We concluded that carbon-14 in neutron-irradiated nuclear graphite is present between the graphite lattice planes as a stable graphite intercalation compound.

Objectives

Worldwide more than 250,000 Mg of neutron-irradiated graphite from nuclear reactors is under storage. Detailed concepts for final disposal or reprocessing of this graphite do not exist up to now.

In a first overview [1] we reported on the possibility to remove tritium and carbon-14 from neutron-irradiated nuclear graphite by thermal treatment. This observation based on a primary investigation of Podruzhina [2] was studied recently in detail by Florjan [3]. However, these studies had only a phenomenological quality. The aim in all cases was the investigation of the general possibility to decontaminate neutron-irradiated graphite from decommissioned nuclear reactors.

From the scientific point of view the reported results lead to the question: Why carbon-14 can be removed from a graphite matrix formed from chemically identical carbon atoms? The only conceivable answer is: Carbon-14 in neutron-irradiated nuclear graphite is present in a chemical bond which is totally different from the graphite lattice bond. Therefore, the main objective of the present work is the experimental analysis of the chemical bond of carbon-14 in nuclear graphite. With this information it will be possible not only to understand the chemical reactions which take place in the graphite decontamination process, but also to ameliorate this decontamination process.

Introduction

Nuclear graphite is a polycrystalline and porous material. In its pore system gases and liquids can adsorb. Additionally during production of reactor graphite heterocyclic compounds containing nitrogen are used to bind the graphite crystallites. The mayor process to create carbon-14 in graphite during neutron irradiation in the reactor is the $^{14}N(n,p)^{14}C$ reaction with a cross section of 77 mb. The recoil energy of the hot carbon-14 atom is 40 keV [4]. This energy is considerably higher than any chemical bond. Hence, the carbon-14 atom will be substantially displaced from its origin to form a new chemical compound in the graphite lattice.

Methods

The determination of the chemical bond of carbon-14 in neutron-irradiated nuclear graphite is a great scientific challenge. The problem is that the amount of carbon-14 in irradiated graphite is only about 1 ppm! An appropriate method for the investigation of the surface chemistry of graphite is the secondary ion mass spectroscopy (SIMS). Chemical elements (isotopes) and molecule groups can be determined up to the ppm or ppb range. In addition, the fragmentation pattern provides information about the chemical environment of the ions appearing in the mass spectrum.

A second method used in this project is the Raman spectroscopy. The Raman spectroscopy permits to observe molecular vibrations. The measured Raman shift provides information about the structure of a molecule. Moreover, material properties like the crystallinity of a solid can be determined. The Raman spectroscopy is the classical method for the spectroscopic investigation of graphite which is IR inactive, as it is well-known.

On account of the low concentration of carbon-14 in neutron-irradiated nuclear graphite we looked for a possibility to produce chemically analogous compounds which should simulate the bond of carbon-14 in graphite with a higher concentration. The appropriate method for this purpose is the implantation of ions. On account of radiation protection reasons and technical conditions an implantation of carbon-14 ions was not possible. Therefore, we implanted carbon-12 and nitrogen-14 ions with the energy of 40 keV. The carbon-12 ions should simulate the entry of carbon-14 in graphite, and the nitrogen-14 ions should verify in which chemical form nitrogen is present in graphite after neutron irradiation in a nuclear reactor.

Graphite samples

For this study we used graphite samples from two different reactor types: 1) neutron-irradiated and virgin fuel pebble graphite from our experimental high temperature pebble bed reactor (AVR) and 2) virgin graphite from the Russian RBMK reactor.

Results and discussion

The secondary ion mass spectroscopy which has a very high mass resolution on account of our time-of-flight mass spectrometer (TOFMS) showed only one signal which could be assigned to carbon-14 (see Fig. 1). This signal with the mass number of 14.003 is very weak. Nevertheless, the high quality of the whole mass spectrum justifies our view that this signal is a real signal. On account of the very low concentration of carbon-14 in graphite a higher signal is also not expected.

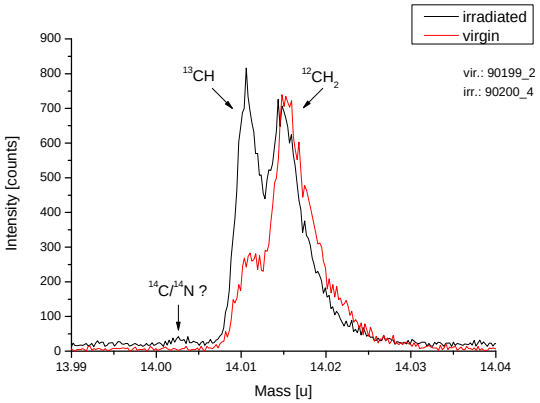

Fig. 1: Mass spectra of irradiated and virgin AVR fuel pebble graphite

Now we had to decide whether the observed signal is assigned to carbon-14 or nitrogen-14. Therefore, we implanted nitrogen-14 to see the mass number at which nitrogen appears in the mass spectrum. We found that the implanted nitrogen appears exclusively as a CN compound with the mass number of 26 (apart from low amounts of C_2N and ^{13}CN). In contrast, no signal was detected at the mass number of 14.003 (see Fig. 2). With this result it is certain that the signal at 14.003 comes really from carbon-14.

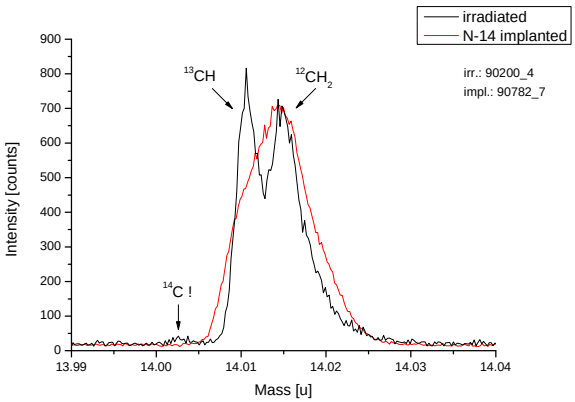

Fig. 2: Mass spectra of irradiated AVR fuel pebble graphite and N-14 implanted RBMK graphite

This investigation still produced another interesting result: The collision of neutrons with nitrogen molecules or nitrogen compounds in nuclear reactors not always leads to a nuclear reaction creating carbon-14 atoms. The generation of highly reactive nitrogen atoms by splitting of the chemical bonds is also possible. These highly reactive nitrogen atoms form very easily chemical bonds to carbon atoms available in graphite in a great quantity.

In Fig. 3 the depth profile of N-14 implanted graphite is shown at the mass number of 26.004. This mass number indicates the presence of CN^- ions. The implantation profile is clearly recognised.

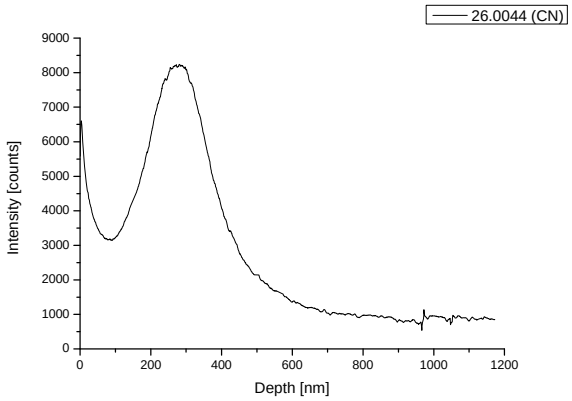

Fig. 3: Depth profile of N-14 implanted RBMK graphite

Also Fig. 4 is noteworthy: The mass spectra of irradiated, virgin and N-14 implanted graphite at the mass number of 26 normalised on the C-12 quantity are shown. It can be seen that the amount of the CN^- ion is significantly higher in irradiated graphite than in virgin graphite. This is caused by the neutron-induced reaction of highly reactive nitrogen atoms with carbon (as described on top).

The amount of CN^- is quite the same in N-14 implanted graphite like in irradiated graphite. That indicates that the same chemical reaction takes place by ion implantation in the laboratory like by neutron irradiation in the nuclear reactor. With this confirmation we see a part of the reactor chemistry and we are able to understand the chemical processes which are caused by the nuclear processes in a nuclear reactor.

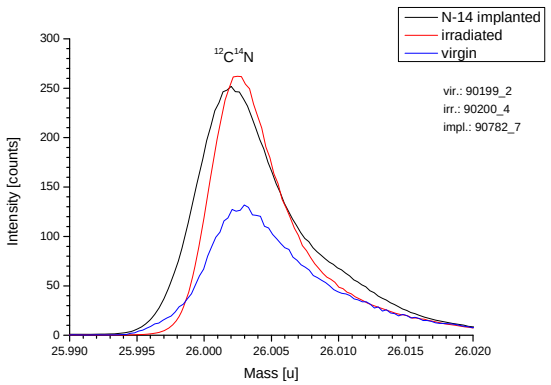

Fig. 4: Mass spectra of irradiated and virgin AVR fuel pebble graphite in comparison to the mass spectrum of N-14 implanted RBMK graphite

The result of the secondary ion mass spectroscopy, namely that carbon-14 appears in the mass spectrum only as an unbound ion, leads to the assumption that carbon-14 is bound in the graphite lattice as an interstitial atom. To verify this assumption the Raman spectroscopy was used.

The Raman spectra of neutron-irradiated and virgin graphite shown in Fig. 5 are sill not expressive enough. One can see the typical peaks of virgin graphite at 1582 cm^{-1} (G band: in-plane vibration of the graphite lattice) and 1358 cm^{-1} (D band: defect structures). In the Raman spectrum of irradiated graphite one can see beside a decrease of the G band and an increase of the D band (decrease of the crystallinity and increase of the disorder) a small leftward shift of both bands which cannot be interpreted immediately.

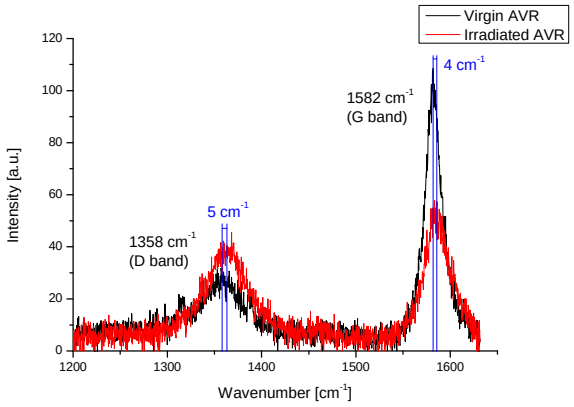

Fig. 5: Raman spectra of irradiated and virgin AVR fuel pebble graphite

Only the implantation of carbon-12 and with it the increase of the amount of the new chemical structures formed by the entry of hot carbon atoms in the graphite lattice brought clarity. In Fig. 6 one can see clearly a significant leftward shift of the Raman bands of the implanted graphite.

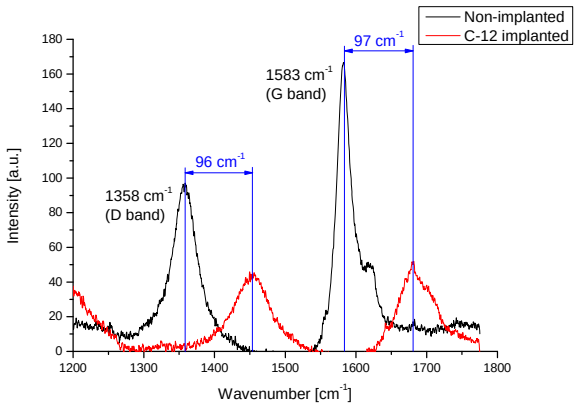

Fig. 6: Raman spectra of C-12 implanted and non-implanted (virgin) RBMK graphite

This leftward shift indicates an increase of the vibration energy of the whole graphite lattice. This can be explained with the fact that the single lattice planes are bonded stronger with each other. The reason for it is that the implanted carbon atoms form stable intercalation compounds between the lattice planes. Such a graphite intercalation compound is shown schematically and as a charge transfer complex in Fig. 7.

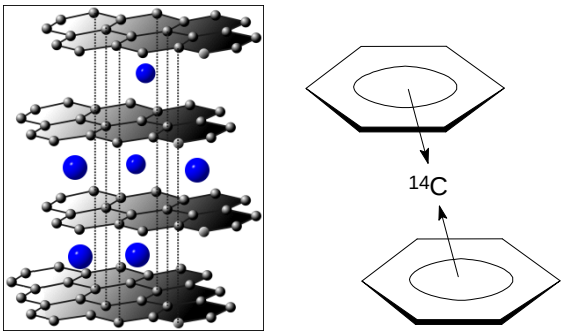

Fig. 7: C-14 bonded in graphite as intercalation compound

With this interpretation the release behaviour of carbon-14 from irradiated graphite can be explained: The graphite intercalation compound is stable enough to not be broken under normal conditions (e.g., in a repository for nuclear waste), but it is less stable than the bond of the carbon atoms in the graphite lattice, so that carbon-14 can be removed from the graphite matrix by suitable chemical reactions (e.g., for the purpose of the decontamination of irradiated graphite).

Acknowledgement
This work is supported by the European Commission (project CARBOWASTE, contract no. FP7-211333).

References

[1] J. Fachinger, W. von Lensa, T. Podruzhina, *Decontamination of nuclear graphite*, Nucl. Eng. Des. 238 (2008) 3086-3091.

[2] T. Podruzhina, *Graphite as radioactive waste: corrosion behaviour under final repository conditions and thermal treatment*, PhD thesis, Rheinisch-Westfälische Technische Hochschule Aachen, 2004.

[3] M. Florjan, *Dekontamination von Nukleargraphit durch thermische Behandlung*, PhD thesis, Rheinisch-Westfälische Technische Hochschule Aachen, 2009.

[4] R. D. Finn, H. J. Ache, A. P. Wolf, *Chemical effects following $^{14}N(n,p)^{14}C$ in magnesium nitride*, J. Phys. Chem. 73 (1969) 3928-3933.

Minor actinide(III) recovery from high active waste solutions using innovative partitioning processes

G. Modolo, A. Geist[1], R. Malmbeck[2]

Institut für Energieforschung, Sicherheitsforschung und Reaktortechnik (IEF-6), Forschungszentrum Jülich GmbH, 52425 Jülich, Germany
[1]Karlsruher Institut für Technologie (KIT) Institut für Nukleare Entsorgung (INE), 76021 Karlsruhe, Germany
[2]European Commission, JRC, Institute for Transuranium Elements (ITU,) 76125 Karlsruhe, Germany
Tel: +49 2461 61 4896, Fax: +49 2461 61 2450, e-mail: g.modolo@fz-juelich.de

Abstract: The selective partitioning of minor actinides from the fission products and separate treatment by transmutation can considerably improve long-term safety of the residual nuclear waste for its subsequent future disposal in a deep underground repository. The present paper will summarize about the ongoing research activities at Forschungszentrum Jülich (FZJ) in the field of actinide partitioning using innovative solvent extraction processes. European research over the last few decades, i.e. in the NEWPART, PARTNEW and the recent EUROPART programs, has resulted in the development of a multicycle process for minor actinide partitioning. In this respect, numerous European partners cooperate closely in European projects. These multicycle processes are based on the co-separation of trivalent actinides and lanthanides (e.g. DIAMEX process), followed by the subsequent trivalent actinide/lanthanide group separation in the SANEX process. Apart from optimizing the properties of the solvent for optimal extraction and separation efficiency, extractant stability is a critical issue to be studied. In this paper, we will focus mainly on the development of flowsheets for the recovery of americium and curium from high active waste solutions, and testing them in centrifugal contactors. The scientific feasibility of the processes developed will be demonstrated on a laboratory scale using synthetic and genuine fuel solution. The future direction of research for the development of new processes within a new European project (ACSEPT) is briefly discussed in the conclusion.

Introduction

Reducing the radiotoxicity of spent nuclear fuel is an important objective to ensure the sustainability of nuclear energy. This objective can be attained by recovering the long-lived elements from the spent fuel constituents and their conversion into short-lived or stable nuclides by irradiation in a dedicated reactor, the so-called partitioning and transmutation strategy (1).

Plutonium, the main contributor to radiotoxicity can already be recovered today by the PUREX process, which with some modifications can also recover neptunium (advanced PUREX). In order to achieve a significant reduction in the radiotoxicity of spent fuel, we must also remove americium and curium. These trivalent minor actinides, however, are not currently industrially separated and they remain with the fission products in the high level liquid waste, which is vitrified and prepared for final disposal. This is not due to a lack of interest in separating these elements but rather due to the fact that they cannot be extracted with tributylphosphate (TBP) within the PUREX process (2). The chemical similarity of trivalent actinides (An) and lanthanides (Ln) combined with the unfavourable mass ratio necessitate very demanding and complex process steps. Processes developed over the last 20 years are predominantly based on the combined extraction of actinides and lanthanides from the PUREX raffinate followed by their subsequent group separation. A distinction is made here between two process variants (1).

In the single-cycle processes, An(III) + Ln(III) are simultaneously separated. Following this, the trivalent actinides are selectively back-extracted (stripped) from the loaded organic phase, e.g. using diethylenetriaminepentaacetic acid (DTPA). The most important developments in terms of this process include the reversed TALSPEAK (USA), DIDPA (Japan) and SETFICS (Japan) processes (2). The multicycle processes, on the other hand, make use of different extractants. Following the joint co-separation of An(III) + Ln(III) from the fission product solution, e.g. using TRUEX (USA), TRPO (China), DIAMEX (France), the next process step involves the joint back-extraction of trivalent An + Ln. This is followed by selective An(III)/Ln(III) separation using a highly selective extractant, e.g. $CyMe_4BTBP$ (3).

The advantage of the latter method is the high purity of the actinide(III) product and a lower volume of secondary waste. This chapter provides an overview of important process developments for actinide separation achieved within the scope of European collaborative projects during the EU 3rd, 4th and 5th Framework Programmes ([4]-[6]). Particular attention will be devoted to developments at Forschungszentrum Jülich, which were made possible through close cooperation with partners in the EU projects. The strategy employed for actinide separation is shown in Figure 1.

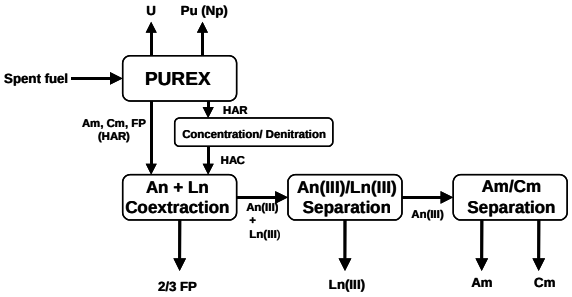

Fig. 1: European partitioning strategy for the separation of all actinides from spent fuel

TODGA-based process developments

In the early 1990s, Stephan et al. ([7]) reported on the extraction of different metals using multidentate ligands such as diglycolamides (DGA). The DGA substance class with an ether group between both amide functions resembles the malonamides and therefore also satisfies the CHON principle. During the late 1990s, Japanese scientists recognized that these ligands are particularly suitable for extracting actinides from acidic waste solutions ([8]).

Extensive extraction studies were performed with this very promising substance class ([9]-[11]). The change from a bidentate ligand (e.g. malonamide) to a tridentate diglycolamide not only significantly increased the affinity for trivalent actinides but also for the lanthanides. Different DGAs were synthesized and the N,N,N´,N´-tetraoctyl-3-oxapentan-diamide (TODGA, Figure 2) was found to have the best properties in terms of extraction, solubility in aliphatic solvents and stability. However, TODGA had a tendency to form a third phase in aliphatic solvents such as n-dodecane, particularly at high metal and HNO_3 concentrations ([12]).

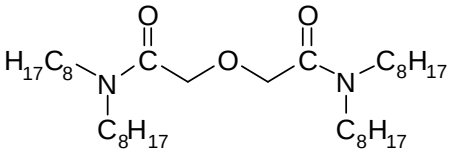

Fig. 2: The structure of TODGA

Within the scope of the PARTNEW project, the aggregation behaviour of TODGA was studied in n-dodecane as a solvent. With the aid of small-angle X-ray and neutron scattering experiments, it was shown that the reason for third-phase formation was the van der Waals interaction at low temperatures ([13]). Other basic studies with TODGA and related compounds can be found in the literature, but almost no studies exist on process development including demonstration. This motivated Modolo et al. to develop a continuous reversible partitioning process, which was successfully tested for the first time in 2003 in centrifugal contactors at Forschungszentrum Jülich ([14]). However, high oxalic acid concentrations of up to 0.4 mol/L were added to the PUREX raffinate in order to suppress the extraction of Zr and Mo on the one hand and third-phase formation on the other hand. At such high oxalic acid concentrations, a slow precipitation of trivalent actinides and lanthanides was observed in the PUREX raffinate. This also led to low oxalate precipitations in the scrubbing steps of the continuous process. This inevitably led to low actinide(III) losses.

Following this, Modolo et al. optimized the partitioning process and suggested a new continuous process in which the extractant was a mixture of 0.2 mol/L TODGA and 0.5 mol/L TBP in TPH ([15]). The addition of TBP not only improved the hydrodynamic properties but also increased the loading capacity of the extractant and reduced the tendency to third-phase formation. In 2006, Forschungszentrum Jülich performed two tests in centrifugal extractors in cooperation with the Institute for Transuranium Elements (ITU) and CEA Marcoule ([16]).

In the second test run (see Figure 3) with 28 stages (4 extraction steps, 12 scrubbing steps and 12 back-extraction steps), 99.99 % of the actinides and lanthanides were selectively extracted and back-extracted from a PUREX raffinate. Problems were caused only by Ru, which was co-extracted (10 % of initial amount) and remained in the spent solvent.

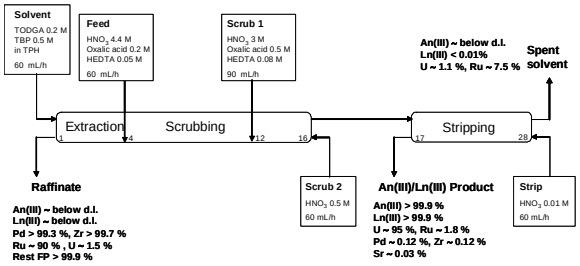

Fig. 3: Flowsheet and main results of the spiked TODGA-based process carried out at FZJ/Jülich in 2006

Based on these positive results, a hot process run was demonstrated at the end of 2006 in ITU's centrifugal extractor battery with almost identical results ([17]). In summary, we can say that the solvent composed of TODGA and TBP in an aliphatic solvent is particularly suitable for separating actinides from a process solution containing numerous fission products. This was demonstrated with a synthetic and a genuine PUREX raffinate with an optimized flowsheet. The main objective (> 99.9 % actinide separation) and a high fission product decontamination were achieved. The results generated are comparable with those for the DIAMEX processes further developed in France and the EU ([17]).

Selective actinide(III)/lanthanide(III) separation

The extraction systems described above separate the trivalent actinides together with the lanthanides from most of the fission products (e.g. Cs, Sr, Mo, Zr, etc.) in the liquid radioactive PUREX raffinate. For the transmutation of the minor actinides, any excess lanthanides (nuclear poison) must once again be separated. As a result of the chemical and physical similarity of both element groups, group extraction is only possible using extractants or complexants containing soft donor atoms, such as N, S, Cl, as they evidently have a stronger interaction with trivalent actinides ([2]).

Many extraction systems with relatively low An(III)/Ln(III) separation factors are described in the literature, but these systems are of little interest for technical application. Systems with a high selectivity are also described, but they are extremely complex (e.g. high salt loads, secondary waste), and they are incompatible with the partitioning processes described previously ([1]).

The SANEX concept (Selective ActiNide EXtraction) which aims to selectively extract trivalent actinides was first proposed by Musikas et al. ([18]). In the early 1980s, the authors discovered two selective An(III)/Ln(III) extraction systems comprising soft N- or S-donor atoms, which subsequently formed the basis for the development of more efficient extractants.

Finally, a new class of heterocyclic N-donor SANEX ligands was developed by Foreman et al. ([19]), namely 6,6´-bis(5,6-dialkyl)-[1,2,4]triazin-3-yl)-[2,2´]bipyridines (BTBPs). A summary of the extraction properties of the reference molecule $CyMe_4BTBP$ (see Figure 4) can be found in Geist et al. ([3]). The slow extraction kinetics were significantly improved with a phase transfer catalyst, such as the malonamide DMDOHEMA.

However, continuous tests on extraction and back-extraction using a single centrifuge showed that even at low process flows, equilibrium values could not be achieved ([20]). Despite this, at the beginning of 2008, a hot test was successfully conducted for this SANEX process with a 16-stage flowsheet at ITU, Karlsruhe ([21]). The product fraction contained more than 99.9 % Am(III) and Cm(III) and less than 0.1 % Ln(III).

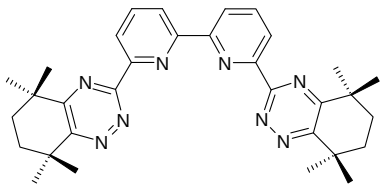

Fig. 4: 6,6´-bis(5,5,8,8-tetramethyl-5,6,7,8-tetrahydro-benzol[1,2,4]-triazin-3-yl)–[2,2´] bipyridine (CyMe4BTBP).

At Forschungszentrum Jülich, Modolo et al. developed an alternative process ([22]). The extractant comprised 0.015 mol/L $CyMe_4BTBP$ in n-octanol. However, instead of 0.25 mol/L DMDOHEMA, only 0.005 mol/L TODGA was used to improve the extraction kinetics. This system showed comparably good extraction properties and the process was successfully demonstrated at Forschungs-zentrum Jülich in February 2008.

In this 20-stage process with 12 extraction steps, 4 scrubbing steps and 4 back-extraction steps, >99.9 % Am(III), Cm(III) and Cf(III) were separated, and the product fraction contained less than 0.1 % of the initial lanthanides (Figure 5).

The hot testing of this process (possibly at ITU, Karlsruhe) is one of the tasks of our collaborative future programme. The SANEX process variant developed at Forschungszentrum Jülich appears to be very promising for two reasons: replacing DMDOHEMA with TODGA increases the solubility of BTBPs, and the regeneration of the extractant is easier.

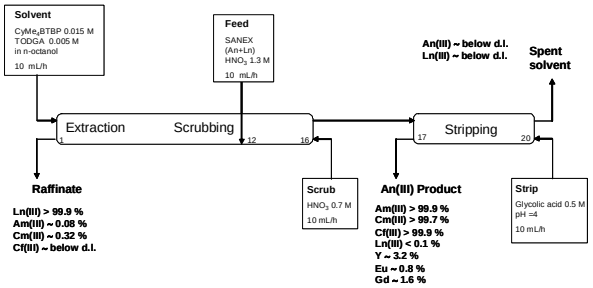

Fig. 5: Flowsheet and main results of the spiked SANEX CyMe4BTBP/TODGA process carried out at FZJ/Jülich in 2008

Americium/curium separation by the LUCA process

The separation of adjacent trivalent actinides represents an even more challenging task than the An(III)/Ln(III) separation. In principal, both elements could be transmuted together in a fast reactor or ADS system. However, because of the high heat decay and neutron emission of curium, any dry or wet fabrication process will require remote handling and continuous cooling in hot cells behind thick concrete shielding. The development of a simple, compact and robust fabrication process appears to be a great challenge ([24]).

Therefore, an effective method for separating Am from Cm prior to re-fabrication is a major prerequisite for the discussion of further fuel cycle scenarios. It is known that separating of americium from curium is a very difficult task due to the very similar properties of these elements. Numerous techniques, including high-pressure ion exchange, extraction chromatography, and solvent extraction using e.g. di(2-ethyl-hexyl)phosphoric acid (HDEHP) have been used for Am(III)/Cm(III) separation and purification ([1], [2]). However, the Am/Cm separation factors were low and did not exceed 3, necessitating a large number of stages in order to obtain a pure product. The best separation of transplutonium elements has been obtained using

methods based on the various oxidation states of the separated elements.

The synergistic mixture (Figure 6) composed of bis(chlorophenyl)-dithiophosphinic acid [$(ClPh)_2PSSH$] and tris(2-ethylhexyl) phosphate (TEHP) shows a very high affinity for actinides(III) over lanthanides(III). Am(III)/Eu(III) separation factors over 3000 are achieved. Surprisingly high Am(III)/Cm(III) separation factors of 6 – 10 were also reported by Modolo et al ([26]). Based on the extraordinary extraction properties of the above mentioned synergistic mixture, the LUCA process ([27]) was invented for the selective recovery of Am(III) from an aqueous nitric acid solution containing trivalent actinides (i.e. Am(III), Cm(III) and Cf(III)) and trivalent lanthanides.

LUCA is the acronym for "Lanthaniden Und Curium Americum separation". Optimization studies were carried out to define the best conditions for extraction, scrubbing and stripping. In addition to the batch extraction studies, a single-stage extraction experiment was conducted to obtain more data on the system kinetics, and to generate data required for the flowsheet calculations.

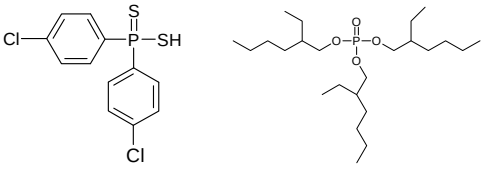

Fig. 6: Synergistic mixture of $(ClPh)_2PSSH$ and TEHP used in the LUCA process

After the data was collected, a 24-stage flowsheet was designed, and the final assessment was performed in a counter-current test using miniature centrifugal contactors ([28]). The results of this counter current test (Figure 13) showed, that the difficult recovery of Am(III) is possible from an acidic solution containing a mixture of trivalent actinides (Am(III), Cm(III) and Cf(III)) and Eu(III) as a lanthanide representative. The LUCA process can be used after a co-extraction process (e.g. after DIAMEX) for the selective extraction of Am(III), leaving Cm(III) together with the lanthanides in the raffinate fraction. Alternatively, the process can also be run after a SANEX process for mutual Am/Cm separation.

In the future, we plan to optimize the formulation of the extractant composition, i.e. by changing the diluent. The promising results obtained here with a surrogate solution should also allow a hot demonstration to be performed in the near future with a genuine process solution. We are confident, that the aromatic dithiophosphinic acids under real process conditions (0.1 - 0.3 mol/L HNO_3, total doses up to 0.5 MGy) are sufficiently stable within the LUCA process. However, at higher acidities (> 0.5 mol/L HNO_3, e.g. during stripping) considerable degradation (by oxidation) of $(ClPh)_2PSSH$ was observed in a former study ([29]). Oxidation of the ligand can be suppressed by adding HNO_2 scavengers or using hydrochloric acid as a stripping medium.

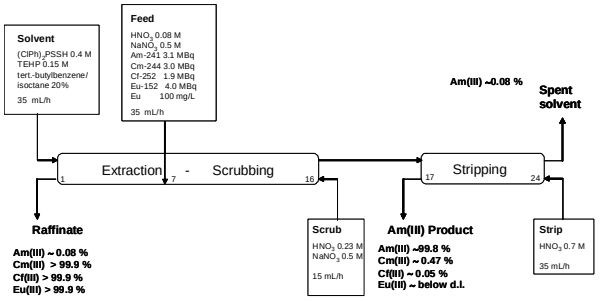

Fig. 7: Flowsheet and main results of the LUCA process for Am/Cm separation carried out at FZJ/Jülich in 2008

Conclusion

Research on partitioning in the European Union (EU) is at such an advanced stage that serious consideration is being given to the industrialization of some separation processes. The leading nation here is France with its ambitious R&D programme on partitioning and transmutation. After decades of research in this area, separating minor actinides (americium and curium) from the PUREX raffinate still poses just as a big a challenge as in the past. The feasibility has already been demonstrated with the aid of a multicycle process (e.g. DIAMEX, TODGA, SANEX) on a laboratory scale using genuine fuel solutions. The challenge now is to optimize the developed processes in terms of their transferability and to work towards industrial process maturity. This will only be possible in the form of a large international project, and is being addressed in the EU follow-on project ACSEPT ([23]).

Within the framework of this international project, the focus is also on developing innovative processes. The objectives include simplifying processes developed in the past and reducing the number of cycles. The direct separation of trivalent actinides from the fission product solution (direct SANEX) is not yet viable as the necessary highly selective and stable extractants are not yet available. However, intensive research is being conducted on their development. Furthermore, tests must be performed to determine whether the processes developed to date are also suitable for future reactor concepts of the third and fourth generation (GEN IV). In some GEN IV concepts, for example, the aim is to jointly recycle all transuranium elements (Np, Pu, Am, Cm). A separation technology adapted for these concepts is therefore essential. Within the framework of the ongoing EU project ACSEPT (2008 - 2012), grouped actinides extraction (GANEX concept) is therefore being studied in order to fulfill the requirements for future issues

Acknowledgement
The author would like to acknowledge the financial support of the European Commission in the projects: NEWPART (FI4I-CT96-0010), PARTNEW (FIKW-CT2000-00087), EUROPART (F16W-CT-2003-508854) and ACSEPT (No. 211267).

References

[1] Actinide and Fission Product Partitioning and Transmutation - Status and Assessment Report, OECD-NEA, Paris, France, 1999.
[2] Nash, K. L. Separation chemistry for lanthanides and trivalent actinides. Chapter 121, in Handbook on the Physics and Chemistry of Rare Earths. Gschneidner, K. A., Jr., Eyring, L., Choppin, G. R., Lander, G. H. Eds. 1994. pp. 197- 235.
[3] Geist, A.; Hill C.; Modolo, G.; Foreman, M.R.St.J.; Weigl, M.; Gompper, K.; Hudson, M.J., Madic C. Solvent Extr. Ion Exch. 2006, 24, 463–483.
[4] Madic, C.; Hudson, M.J.; Liljenzin, J.O.; Glatz, J.P.; Nannicini, R.; Facchini, A.; Kolarik, Z., Odoj, R. New partitioning techniques for minor actinides, European report, EUR 19149, 2000.
[5] Madic, C.; Testard, F.; Hudson, M.J.; Liljenzin, J.O.; Christiansen, B.; Ferrando, M.; Facchini, A.; Geist, A.; Modolo, G.;Gonzales-Espartero, A.; De Mendoza, J., PARTNEW- New Solvent Extraction Processes for Minor Actinides-Final Report, CEA-report 6066, 2004.
[6] C. Madic, M.J. Hudson, P. Baron, N. Ouvrier, C. Hill, F. Arnaud, A. G. Espartero, J.-F. Desreux, G. Modolo, R. Malmbeck, S. Bourg, G. De Angelis, J.Uhlir EUROPART. European Research Programme for Partitioning of Minor Actinides within High Active Wastes Issuing from the Reprocessing of Spent Nuclear Fuels, Proceedings of the FISA 2006, Luxembourg, 2006.
[7] H. Stephan, K. Gloe, J. Beger, P. Mühl, Solvent Extr. Ion Exch. 1991, 9(3), 459-469.
[8] Y. Sasaki, G.R. Choppin, Anal. Sci. 1996, 12, 225-230.
[9] Sasaki, Y., Choppin, G.R. Radiochim. Acta 1998, 80, 85–88.
[10] Sasaki, Y., Sugo, Y., Suzuki, S., Tachimori, S. Solvent Extr. Ion Exch. 2001, 19, 91–103.
[11] S. Tachimori, Y. Sasaki, S. Suzuki Solvent Extr. Ion Exch. 2002, 20(6), 687-699.
[12] Yaita, T., Herlinger, A.W., Thiyagarajan, P., Jensen, M.P. Solvent Extr. Ion Exch. 2004, 22, 553-571.
[13] Nave, S., Modolo, G., Madic, C., Testard, F. Solvent Extr. Ion Exch. 2004, 22(4), 527-551.
[14] Modolo, G., Vijgen, H., Schreinemachers, C., Baron, P., Dinh, B. TODGA Process Development for Partitioning of Actinides(III) from PUREX Raffinate, Proceedings of GLOBAL 2003, New Orleans, Louisiana, USA, 2003.
[15] Modolo, G., Asp, H., Schreinemachers, C., Vijgen, H. Solvent Extr. Ion Exch. 2007, 25, 703-721.
[16] Modolo, G., Asp, H., Vijgen, H., Malmbeck, R., Magnusson, D., Sorel, C. Solvent Extr. Ion Exch. 2008, 26 (1), 62 – 76.
[17] Magnusson, D.; Christiansen, B.; Glatz, J.-P.; Malmbeck, R.; Modolo, G.; Serrano-Purroy, D.; Sorel, C. Solvent Extr. Ion Exch. 2009, 27 (1), 26-35
[18] Musikas, C., Vitorge, P., Pattee, D. Progress in trivalent actinide lanthanide group separation. Proceedings of Internat. Solvent Extr. Conf (ISEC' 83). 1983.
[19] Ekberg, C., Fermvik, A., Retegan, T., Skarnemark, G., Foreman, M. R. S., Hudson, M. J., Englund, S., Nilsson, M. Radiochimica Acta 2008, 96(3-4), 225–233.
[20] Magnusson, D., Christiansen, B., Glatz, J.-P., Malmbeck, R., Modolo, G., Serrano-Purroy, D. Sorel, C. Radiochimica Acta, 2009, 97 (3), 155-159.
[21] Magnusson, D.; Christiansen, B.; Foreman, M.R.S.; Geist, A.; Glatz, J.-P.; Malmbeck, R.; Modolo, G.; Serrano-Purroy, D.; Sorel,C. Solvent Extr. Ion Exch. 2009, 27 (2), 97-106.
[22] Modolo, G.; Sypula, M.; Geist, A.; Hill, C.; Sorel, C.; Malmbeck, R.; Magnusson, D.; Foreman, M. R. St. J, Development and demonstration of a new SANEX process for actinide(III)-lanthanide(III) separation using a mixture of CyMe4BTBP and TODGA as selective extractant, Proceedings of the 10th OECD/NEA P&T meeting, Mito, Japan, 2008.
[23] S. Bourg, C. Caravaca, C. Ekberg, C. Hill, C. Rhodes ACSEPT, Toward the Future Demonstration of Advanced FuelTreatments, Proceedings of Global 2009, Paris, France, 2009.
[24] Pillon, S., Somers, J., Grandjean, S., Lacquement, J. J. Nucl. Mater. 2003, 320, 36-43.
[25] Modolo, G., Odoj, R., Solvent Extr. Ion Exch. 1999, 17 (1), 33-53.
[26] Modolo, G., Nabet, S. Solvent Extr. Ion Exch. 2005, 23, 359-373.
[27] Modolo, G., Odoj, R. Method for separating trivalent americium from trivalent curium. European patent EP 1664359B1, 03.01.2007.
[28] Modolo, G., Kluxen, P., Geist, A., Radiochimica Acta, 2010, 98, 193-201.
[29] Modolo, G., Seekamp, S. Solvent Extr. Ion Exch. 2002, 20(2), 195-210.

1-cycle SANEX process development studies for direct recovery of trivalent actinides from PUREX raffinate

A. Wilden, M. Sypula, C. Schreinemachers, P. Kluxen, G. Modolo

Institut für Energieforschung, Sicherheitsforschung und Reaktortechnik (IEF-6)
Forschungszentrum Jülich GmbH, 52425 Jülich, Germany
Tel: +49(0)2461613965, Fax: +49(0)2461612450
Corresponding author: a.wilden@fz-juelich.de

Abstract: The direct selective extraction of trivalent actinides from a simulated PUREX raffinate solution (1-cycle SANEX) was studied using a mixture of $CyMe_4BTBP$ and TODGA. The solvent showed a high selectivity for trivalent actinides with a high lanthanide separation factor. However the coextraction of some fission products, such as Cu, Ni, Zr, Mo, Pd, Ag and Cd was observed. The extraction of Zr and Mo could be suppressed using oxalic acid but the use of the well-known Pd complexant HEDTA was unsuccessful. During screening experiments with different amino acids, the sulphur-bearing amino acid L-Cysteine showed good complexation of Pd and prevented its extraction into the organic phase without influencing the extraction of trivalent actinides. A strategy for a single-cycle process is proposed within this paper.

Introduction

The development of new and innovative processes for the processing of spent nuclear fuel solutions is a very intensively studied topic in nuclear research all over the world [1, 2]. As the liquid aqueous waste solution from reprocessing contains approx. 40 different elements in concentrations ranging from a few milligrams up to several grams per litre, the selective separation of trivalent actinides from this multi-element solution is one of the most challenging problems. The separation of the trivalent actinides from the lanthanides is a particularly difficult step, as the two groups of f-elements have very similar physical and chemical properties.

In Europe, the DIAMEX-SANEX (DIAMide EXtraction - Selective ActiNide EXtraction) partitioning process is one of the most promising strategies, which is foreseen to be converted from lab scale to industrial scale. The first step of this process (DIAMEX) uses a diamide extractant to coextract lanthanides and minor actinides from the highly acidic PUREX-raffinate [3, 4]. In the subsequent step (SANEX), the trivalent actinides are separated from the lanthanides e.g. by the highly selective $CyMe_4BTBP$ extractant [5, 6]. A drawback of such a process design is the need for two separate processes using two different ligands. Within the current European project ACSEPT (Actinide reCycling by SEParation and Transmutation), a new process design is envisaged, the so-called "innovative SANEX" concept. In this strategy, the trivalent actinides and lanthanides are coextracted in a DIAMEX-type process. Then, the loaded solvent is subjected to several stripping steps. The first one concerns selectively stripping the trivalent actinides with selective water-soluble ligands followed by the subsequent stripping of trivalent lanthanides [7].

A more challenging route studied within this paper is the direct actinide (III) separation from the PUREX raffinate using a mixture of $CyMe_4BTBP$ and TODGA (structures shown in Fig. 1) as extractants, the so-called 1-cycle SANEX process. A single process directly using the PUREX raffinate would reduce the number of cycles, thus saving the DIAMEX process, making the complete advanced reprocessing process more economical and easier.

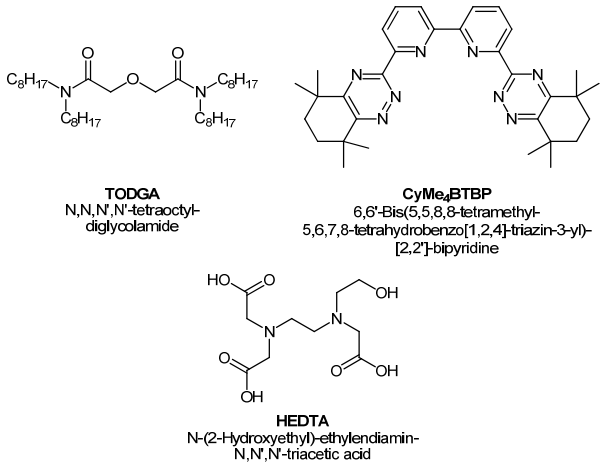

Fig. 1: Structures of TODGA, $CyMe_4BTBP$ and HEDTA.

Geist et al. have shown the $CyMe_4BTBP$ molecule to be a very selective extractant for the separation of actinides from lanthanides [8]. Magnusson et al. demonstrated the performance of $CyMe_4BTBP$ in a hot SANEX test using 0.25 mol/L of the malonamide DMDOHEMA as phase transfer catalyst [5]. The use of a phase transfer catalyst is necessary owing to the slow kinetics of the $CyMe_4BTBP$-molecule which can be significantly improved by the use of DMDOHEMA. Modolo et al. recently proposed that 0.25 mol/L DMDOHEMA can be substituted with 0.005 mol/L TODGA [9]. This system shows comparably good extraction properties and kinetic behaviour compared to DMDOHEMA, and the performance of the system was demonstrated in a spiked test. Both experiments used a DIAMEX raffinate

solution containing actinides and lanthanides as a SANEX feed solution for the experiments. After a 20-stage counter-current process, an actinide product fraction containing >99.9% of the actinides with less than 0.1% lanthanides was obtained. Despite these very successful tests, the question arose as to whether it would be possible to directly and selectively extract the actinides from a PUREX raffinate solution leaving the lanthanides and the other fission products in the aqueous phase.

Results and discussion

Batch extraction studies were carried out with a synthetic PUREX raffinate. An organic phase consisting of 0.015 mol/L $CyMe_4BTBP$ and 0.005 mol/L TODGA diluted in a mixture of TPH and 1-Octanol (40/60 v/v) was used as extractant. The composition of the synthetic PUREX raffinate solution and the corresponding distribution ratios of the elements for the extraction without adding any complexants are given in Table 1 (see column 3).

Table 1. The extraction of actinides and fission products from a simulated PUREX-raffinate with $CyMe_4BTBP$/TODGA.

Solute	Concentration [mg/L or as shown]	Without complexant	$C_2H_2O_4$	HEDTA	$C_2H_2O_4$ + HEDTA
		Distribution ratio			
^{241}Am	trace amounts	10.8	9.1	14.8	9.4
^{244}Cm	trace amounts	4.3	3.6	6.1	3.8
Y	90	0.04	0.85	0.15	0.73
La	239	<0.01	0.02	0.01	0.01
Ce	567	<0.01	0.03	0.01	0.02
Pr	223	0.01	0.04	0.02	0.03
Nd	718	0.02	0.06	0.04	0.05
Sm	149	0.07	0.14	0.10	0.13
Eu	34	0.16	0.24	0.14	0.25
^{152}Eu	trace amounts	0.06	0.22	0.10	0.20
Gd	51	0.08	0.17	0.08	0.15
Ni	40	30.0	18.4	32.1	37.3
Cu	19	4.88	15.7	19.1	5.60
Zr	1071	0.50	0.01	0.23	0.01
Mo	678	2.57	0.21	3.76	0.18
Pd	168	6.19	8.81	6.63	4.69
Ag	12	0.88	2.48	3.59	0.51
Cd	15	12.3	6.92	14.2	4.03
Cr	93	0.02	0.03	0.03	0.04
Sn	11	0.12	0.31	0.46	0.05
Sb	4.6	0.12	0.07	0.09	0.08
Rb	63	0.08	0.10	0.11	0.09
Ru	356	0.09	0.07	0.10	0.05
Rh	73	<0.01	<0.01	<0.01	<0.01
Te	165	0.03	<0.01	0.01	<0.01
Sr	177	<0.01	<0.01	0.01	<0.01
Ba	259	<0.01	<0.01	<0.01	<0.01
Cs	542	<0.01	<0.01	<0.01	<0.01
Al	2	n.d.	n.d.	n.d.	n.d.
Fe	1900	n.d.	n.d.	n.d.	n.d.
Se	10	n.d.	n.d.	n.d.	n.d.
Na	1600	n.d.	n.d.	n.d.	n.d.
HNO_3	3.2 mol/L				

n.d.: not determined.

These preliminary results show that the direct extraction of Am and Cm from a synthetic PUREX raffinate solution is possible with good extraction of the actinides and a high separation factor of Am/Eu of 68. However, some non-lanthanide fission products were coextracted with the actinides, namely Zr, Ag, Cd, Mo, Ni, Cu and Pd. Zirconium and molybdenum play a major role, because their concentration in the PUREX-raffinate solution is very high (1071 and 678 mg/L, respectively). Even a relatively low distribution ratio in this case leads to a considerable loading of the organic phase, thereby reducing the free extractant concentration available for the actinide extraction. Palladium (168 mg/L) must also be considered due to the higher concentration, whereas Ag (12 mg/L), Cd (15 mg/L), Ni (40 mg/L) and Cu (19 mg/L) are contained in smaller amounts.

The coextraction of Zr, Mo and Pd is a problem that was often overcome by the use of complexing agents, namely oxalic acid and HEDTA (Fig. 1) in experiments concerning the DIAMEX process [10].

Table 1 shows the results for the addition of oxalic acid. It shows that the distribution ratios of Zr and Mo are reduced significantly by oxalic acid, as expected. The extraction behaviour of Ag, Cd, Ni, Cu and Pd is not affected very much by oxalic acid and the results furthermore show that Y is extracted much better due to the lower overall loading of the organic phase.

Table 1 also shows the results for experiments with the addition of HEDTA alone, and those with a mixture of oxalic acid and HEDTA. The experiment with HEDTA alone shows that the Zr distribution ratio is approximately halved compared to the experiment without the addition of complexants, but there is no influence on the extraction of Pd. This was not expected and experiments with Pd single-element solution showed no influence of the HEDTA concentration on the extraction of Pd. The experiment with a mixture of oxalic acid and HEDTA shows that the addition of HEDTA is not advantageous compared to the experiment with oxalic acid alone and that the use of HEDTA can be omitted.

The aim of this work was to find a suitable masking agent for Pd. A number of amino acids and some amino acid derivatives were therefore tested for their influence on the Pd distribution ratio, together with ^{241}Am and ^{152}Eu. An overview of the tested complexants is shown in Fig. 2. Amino acids were chosen because of their relatively complex coordination chemistry due to the presence of different donor atoms (O, N, S) in diverse structural constitutions thus allowing different chelate ring sizes, and because of their well solubility in aqueous solutions.

They were all tested in two concentrations, 0.1 and 0.2 mol/L. The results of the test with 0.1 mol/L amino acid are shown in Fig. 3. The results of the test with 0.2 mol/L amino acid show a similar behaviour and therefore are not shown.

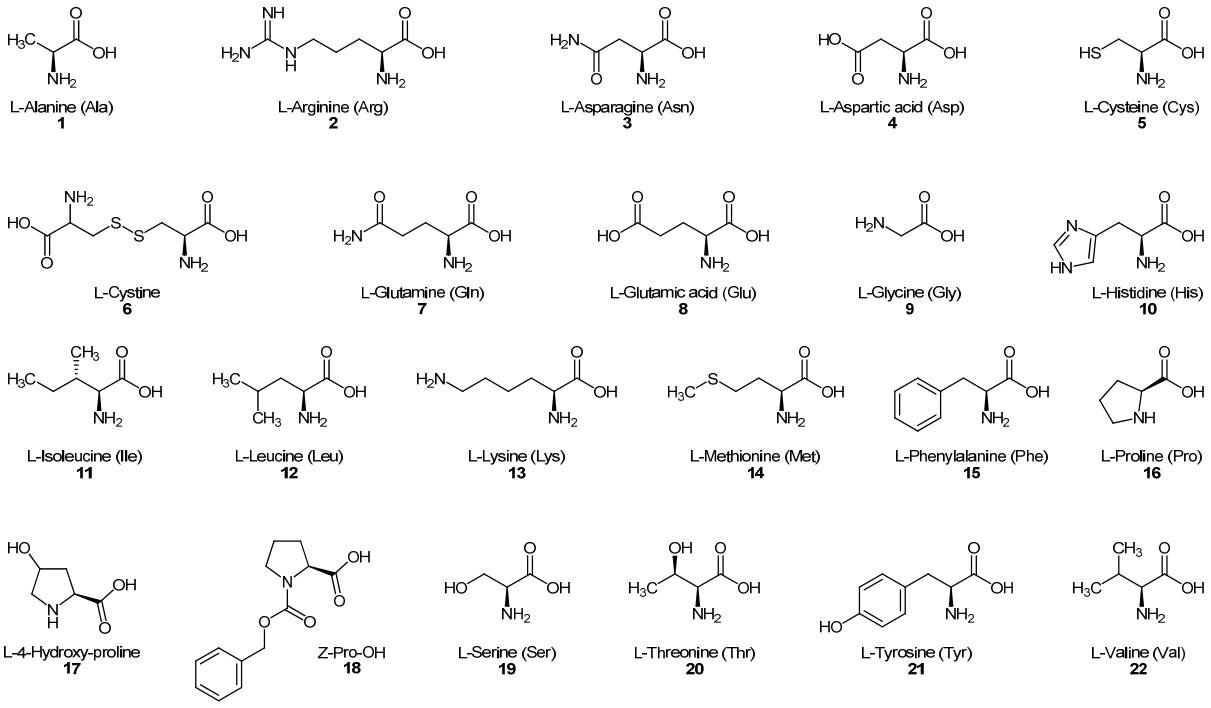

Fig. 2: Overview of the tested amino acids and derivatives.

Just two of the 22 tested amino acids showed a significant influence on the distribution ratio of Pd: L-Cysteine **5** and L-Cystine **6** (structures are shown in Fig. 2). The Pd distribution ratios are reduced considerably and reach values below 1. Furthermore, they had no influence on the extraction of Am(III) and Eu(III). The distribution ratios of Am(III) and Eu(III), as well as the separation factor, remained unchanged. L-Cysteine was chosen for further studies, because of the structural similarity of the two molecules. L-Cystine is a dimer of two L-Cysteine molecules.

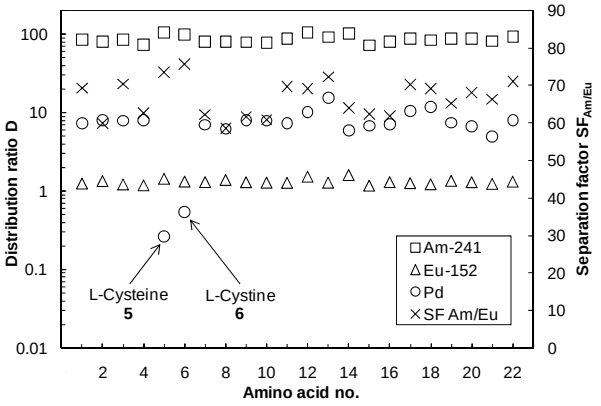

Fig. 3: Amino acid screening using $CyMe_4BTBP$ + TODGA in TPH/1-Octanol = 40/60 and different amino acids in 3 mol/L HNO_3 as aqueous phases.

The 1-cycle SANEX process is intended to be used to separate the minor actinides from a PUREX-raffinate solution. To test the new complexant under process relevant conditions a simulated PUREX-raffinate solution had been prepared with the composition shown in Table 1.
In the following batch experiments, a process-like extraction series was used. The composition of the aqueous phases is shown in Table 2.

Table 2: Composition of the aqueous phases used in the first experiment.

concentration / mol/L	Step 1: Ex	Step 2: Scrub I	Step 3: Scrub II	Step 4: Strip
HNO_3	3.2	1.0	1.0	0.01
oxalic acid	0.3	0.2		
L-Cysteine	0.05	0.05		

In the first step, the extraction step, 4 mL of the simulated PUREX-raffinate solution were contacted for 15 min. with 4 mL of a freshly prepared organic phase with the same composition as in the previous experiments (0.015 mol/L $CyMe_4BTBP$ + 0.005 mol/L TODGA in TPH/1-Octanol = 40/60). After phase separation, aliquots of each phase were taken for analysis and 3.0 mL of the remaining organic phase were contacted with 3.0 mL of a freshly prepared aqueous phase (Scrub I). Again after phase separation, aliquots of each phase were taken for analysis and 2.0 mL of the remaining organic phase were contacted with 2.0 mL of a freshly prepared aqueous phase (Scrub II). In the last step, called Strip, 1.0 mL of the separated organic phase was contacted with 1.0 mL of a freshly prepared aqueous phase.
During this first extraction experiment, L-Cysteine caused a voluminous precipitation, which is unwanted in a counter-current process. Therefore, the extraction series was altered as shown in Table 3. The experiment was conducted as described above.

Table 3: Composition of the aqueous phases used in the second experiment.

concentration / mol/L	Step 1: Ex	Step 2: Scrub I	Step 3: Scrub II	Step 4: Strip
HNO_3	3.2	1.0	1.0	0.01
oxalic acid	0.3	0.2		
L-Cysteine			0.01	

During this experiment, no precipitate formed and no third phase formation was observed. Fig. 4 shows that americium and curium are well extracted and that they stay in the organic phase during the washing steps. In the last step (Strip), they were back extracted into the aqueous phase. The trivalent lanthanides were not extracted well (with the highest distribution ratios for Europium) and therefore a high separation between the trivalent lanthanides and the actinides was achieved. The good back-extraction behaviour of the $CyMe_4BTBP$ system is advantageous for the development of a reversible process with recycling of the organic phase which could be reused after a possible solvent treatment.

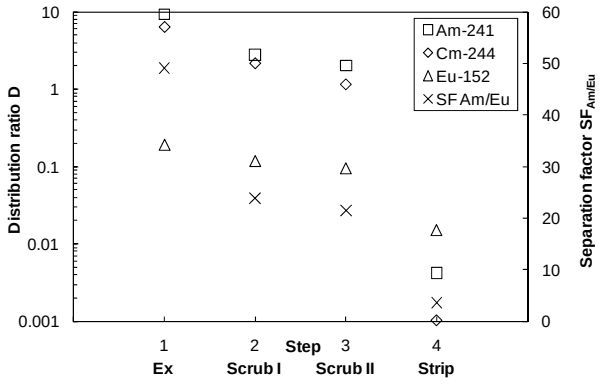

Fig. 4: Distribution ratios and separation factor of ^{241}Am, ^{244}Cm and ^{152}Eu in a simulated four-step process using $CyMe_4BTBP$ + TODGA in TPH/1-Octanol = 40/60 and aqueous phases as shown in Table 3.

Fig. 5 shows the results from ICP-MS analysis for some selected inactive elements. In this figure, the concentration of the elements in the organic phase is depicted instead of the distribution ratio because the D-values of copper and nickel could not be determined due to their low concentration in the aqueous phase. The results show that copper and nickel are nearly completely extracted and that they stay in the organic phase during the whole experiment. They could possibly be scrubbed in an alkaline solvent treatment, but this topic was not investigated during this work. The extraction of zirconium and molybdenum was prevented by the use of oxalic acid and yttrium was scrubbed during the first two steps. Furthermore, the results show that palladium and silver were effectively scrubbed from the organic phase in the third step, the section with L-Cysteine addition.

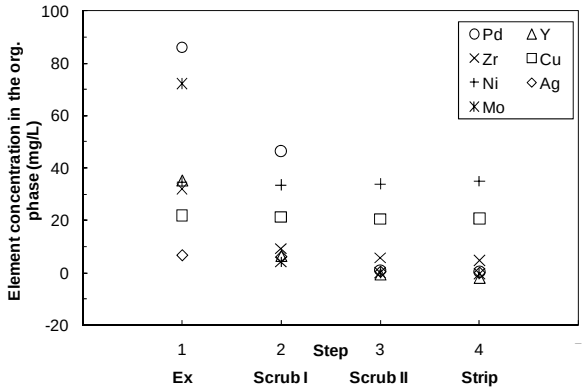

Fig. 5: Organic phase concentrations of selected stable elements as determined by ICP-MS in a simulated four-step process using $CyMe_4BTBP$ + TODGA in TPH/1-Octanol = 40/60 and aqueous phases as shown in Table 3.

Conclusion

In this work, it was shown that the direct and selective extraction of trivalent actinides from a synthetic PUREX raffinate solution as 1-cycle SANEX seems to be possible. Distribution ratios for trivalent actinides and the separation factor from the trivalent lanthanides were high. Nonetheless the reported system suffered from the coextraction of some of the non-lanthanide fission product elements.

22 amino acids and derivatives were tested and L-Cysteine showed good complexation behaviour of Pd, without influencing the extraction of trivalent actinides. In a process-like extraction series, the practicability of the use of L-Cysteine as complexant for Pd and Ag was shown.

The high distribution ratios of Ni and Cu could be problematic for a continuous working industrial process. More investigations have to be done to examine stripping conditions for these elements. A possible solvent cleanup step has to be developed for the design of an industrial process.

Acknowledgements

Financial support for this research was provided by the European Commission (project ACSEPT – Contract No. FP7-CP-2007-211 267). M. R. S. Foreman, University of Reading, is greatly acknowledged for providing $CyMe_4BTBP$.

References

[1] M. Nilsson, K. L. Nash, Solvent Extr. Ion Exch. 25 (2007) 665-701.

[2] C. Ekberg, A. Fermvik, T. Retegan, G. Skarnemark, M. R. S. Foreman, M. J. Hudson, S. Englund, M. Nilsson, Radiochim. Acta 96 (2008) 225-233.

[3] O. Courson, M. Lebrun, R. Malmbeck, G. Pagliosa, K. Romer, B. Satmark, J. P. Glatz, Radiochim. Acta 88 (2000) 857-863.

[4] R. Malmbeck, O. Courson, G. Pagliosa, K. Romer, B. Satmark, J. P. Glatz, P. Baron, Radiochim. Acta 88 (2000) 865-871.

[5] D. Magnusson, B. Christiansen, M. R. S. Foreman, A. Geist, J. P. Glatz, R. Malmbeck, G. Modolo, D. Serrano-Purroy, C. Sorel, Solvent Extr. Ion Exch. 27 (2009) 97-106.

[6] D. Magnusson, B. Christiansen, J.-P. Glatz, R. Malmbeck, G. Modolo, D. Serrano-Purroy, C. Sorel, Radiochim. Acta 97 (2009) 155-159.

[7] X. Hérès, C. Sorel, M. Miguirditchian, B. Camès, C. Hill, I. Bisel, D. Espinoux, C. Eysseric, P. Baron, B. Lorrain, Proc. of the GLOBAL 2009, Paris, France (2009) 9384.

[8] A. Geist, C. Hill, G. Modolo, M. R. S. J. Foreman, M. Weigl, K. Gompper, M. J. Hudson, C. Madic, Solvent Extr. Ion Exch. 24 (2006) 463-483.

[9] G. Modolo, M. Sypula, A. Geist, C. Hill, C. Sorel, R. Malmbeck, D. Magnusson, M. R. S. J. Foreman, Proc. of the Tenth Information Exchange Meeting on Actinide and Fission Product Partitioning and Transmutation, Mito, Japan (2008).

[10] D. Serrano-Purroy, P. Baron, B. Christiansen, R. Malmbeck, C. Sorel, J. P. Glatz, Radiochim. Acta 93 (2005) 351-355.

Separation of An(III) from PUREX raffinate as an innovative SANEX process based on a mixture of TODGA/TBP

M. Sypula, A. Wilden, C. Schreinemachers, G. Modolo

Institut für Energieforschung, Sicherheitsforschung und Reaktortechnik (IEF-6)
Forschungszentrum Jülich GmbH, 52425 Jülich, Germany
Tel: +49(0)2461 616282, Fax: +49(0)2461 612450
Corresponding author: m.sypula@fz-juelich.de

Abstract: Within the new European project ACSEPT devoted to partitioning and transmutation of minor actinides, new approaches for minor actinides separation were proposed. One of the new concepts, namely innovative SANEX process based on TODGA/TBP for selective An(III) separation from PUREX raffinate was studied. This process combines DIAMEX process (co-extraction of An + Ln) and SANEX process (selective actinide extraction), thus only one extractant can be used (simplicity). Oxalic acid usually used for Zr complexation was considered a weak point. An investigation to substitute oxalic acid with a different masking agent was carried out. A new masking agent already studied in FZJ was applied and showed good complexation properties towards Zr and Pd. Re-investigation of the formula of the actinide stripping solution was also performed. Good separation of Ln over Am was obtained by means of DTPA and citric acid. Glycine appeared to be the strongest within the tested buffers.

Introduction

Several processes for recycling nuclear spent fuel have been designed and tested but only the PUREX process (U, Pu and Np recovery) has been employed on an industrial scale. After the partitioning step, Pu and U can be transferred back to the nuclear reactors as MOX fuel (mixed oxide). Recovered minor actinides can be converted into short-lived nuclides in advanced reactors (transmutation).

Within the ACSEPT project, a new innovative SANEX process (i-SANEX) combining two other separate processes, namely DIAMEX and SANEX, was investigated. This process based on a well known ligand TODGA consists of:

1. Co-extraction of Ln(III) and An(III) from PUREX raffinate by a mixture of TODGA (*tetraoctyl-diglycolamide*) and TBP (*tributyl phosphate*) dissolved in TPH (*total petroleum hydrocarbon*).
2. Selective stripping of An(III) by polyaminocarboxylic acid (complexing agent) and carboxylic acid (buffer).
3. Stripping of Ln(III).

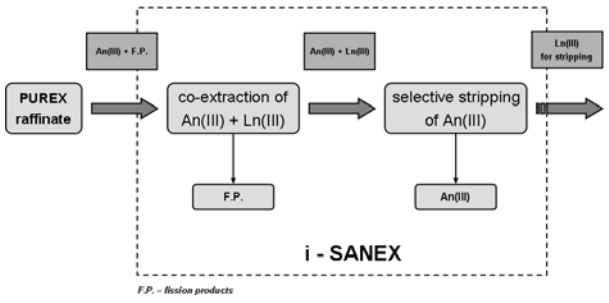

Fig. 1: Innovative SANEX concept for separation of An(III) from PUREX raffinate.

N,N,N',N'-tetraoctyl diglycolamide (TODGA) was chosen as an extractant for co-extraction of An(III) + Ln(III). This ligand (Figure 2) has very strong affinity towards An(III) and Ln(III) with distribution ratios over 300. Moreover, its high hydrolytic and radiolytic stability makes it an ideal extractant for nuclear purposes. Nevertheless, high loading of the organic solvent with metals causes formation of the third phase making it inapplicable in a continuous process. Modolo et al. [1] studied the influence of tributylphosphate (TBP, Figure 2) on suppression of the third phase formation. It has been found that 0.5 mol/L TBP added to the solvent acts as an organic phase modifier increasing the limiting organic concentration (LOC) up to 0.02 mol/L of Nd [1].

In our experiments the solvent consisted of 0.2 mol/L TODGA + 0.5 mol/L TBP dissolved in TPH.

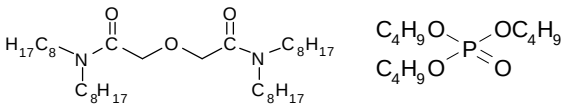

Fig. 2: The chemical structures of the solvent components.

Due to the very high extraction strength of TODGA, some of the fission products were co-extracted together with An(III) + Ln(III). Modolo et al. [1] overcame this problem by applying oxalic acid and N-(2-hydroxyethyl) ethylenediaminetriacetic acid (HEDTA) to suppress the extraction of Zr and Pd, respectively. High concentration of oxalic acid can cause slow precipitation of An(III) and Ln(III) therefore we decided to use cyclohexanediaminetetraacetic acid (CDTA) (Figure 3) to keep Zr and Pd in the aqueous phase. This hydrophilic complexing agent was studied previously by us and showed a very good complexation ability towards Zr and Pd.

Very similar studies were done by CEA resulting in cold and spiked counter-current tests run [2]. However,

the co-extraction and scrubbing steps in CEA process contained oxalic acid and HEDTA as masking agents. Heres et al. pointed out a very high sensitivity of the An(III) stripping step in the process towards pH. It is well known that TBP extracts HNO_3 thus in the extraction step nitric acid is partly extracted to the organic phase by the mixture TODGA/TBP. The extracted nitric acid is stripped into the aqueous phase in the An-stripping step decreasing the pH of the stripping solution and the Ln/An separation efficiency. To minimise pH changes an addition of a buffer is needed into the stripping solution.

TODGA itself possesses higher affinity towards Ln(III) than An(III), the separation between those two elements can be enhanced by means of a hydrophilic complexing agent i.e. HEDTA or DTPA.

The last step in this process is the stripping of Ln(III) with low concentrated nitric acid.

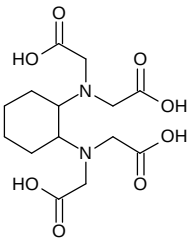

CDTA

Fig. 3: The chemical structure of the masking agent.

Results and discussion

The exemplary flow-sheet of this process (Figure 4) is based on the flow-sheet for co-extraction of An(III)+Ln(III) from a PUREX raffinate [3].

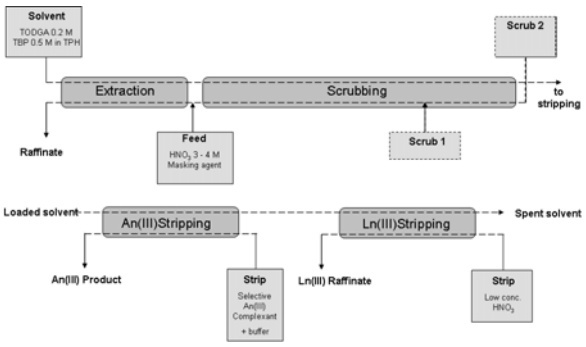

Fig. 4: An exemplary flow-sheet for An(III) separation from PUREX raffinate.

All the sections of the process were studies separately in batch tests to find the right conditions, nevertheless the single centrifuge-contactor tests together with full spiked run are planned in the future.

Table 1 shows the distribution ratios of the appropriate elements in the extraction step.

Table 1: The distribution ratios of the elements in the extraction step.

Element	Distribution ratio	Element	Distribution ratio
^{241}Am	>100	Mo	0.121
Y	60	Ru	0.338
La	46	Sr	1.88
Ce	63	Ba	0.038
Pr	73	Cr	0.011
Nd	80	Cs	<0.01
Sm	71	Cu	<0.01
Eu	41	Ni	<0.01
^{152}Eu	>100	Sn	<0.01
Gd	43	Rb	0.093
Zr	0.010	Rh	<0.01
Pd	0.30	Te	<0.01
Cd	0.062		

As we see in the Table 1, the extraction of Zr and Pd is suppressed by CDTA. The distribution ratios for Zr and Pd without a masking agent are 45 and 4, respectively. ^{241}Am which represents An(III) is quantitatively extracted by TODGA together with Ln(III). Concerning the fission products only Sr, Mo and Ru are partly extracted. The content of the first two elements in the organic phase might be possibly decreased by implementing additional scrubbing step(s) with various nitric acid concentration. Ruthenium once being extracted is expected to stay in the organic phase through the whole scrubbing section, although it might be possible to separate it from the An(III) by adjusting the An stripping conditions.

In the An-stripping section our studies were focused on the selection of an appropriate buffer together with a selective An complexant. The criterion for buffer was the best stabilising properties at certain pH, while for the complexant the highest Ln/An separation factor possible. Some of the distribution ratios of Eu were bellow 1 (Figure 5), although they can be increased by means of the nitrate ions in the stripping solution.

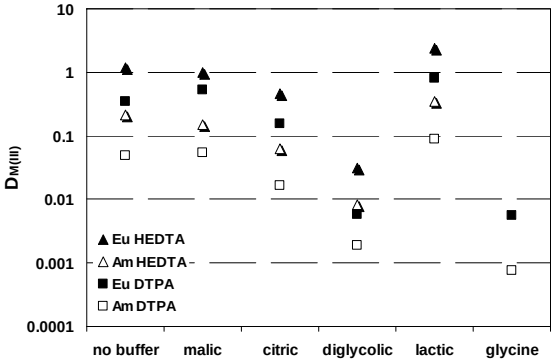

Fig. 5: The distribution ratios of ^{241}Am and ^{152}Eu for different buffers and complexing agents.

When glycine (Figure 6a) was used, the change of the pH comparing the aqueous phase before and after stripping was the smallest (Figure 7), although by using citric acid (Figure 6b) the $SF_{Eu/An}$ was the highest (Figure 8).
Diethylenetriaminepentaacetic acid (DTPA, Figure 6c) gave the highest separation factor from all tested complexants.

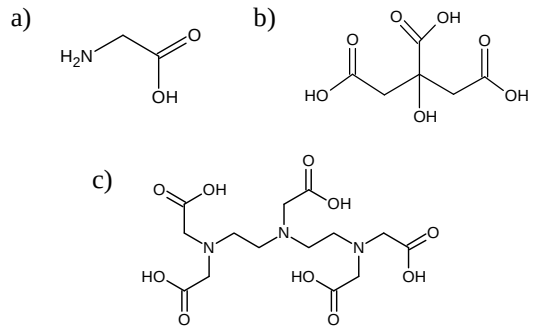

Fig. 6: The chemical structures of **a)** glycine, **b)** citric acid and **c)** DTPA.

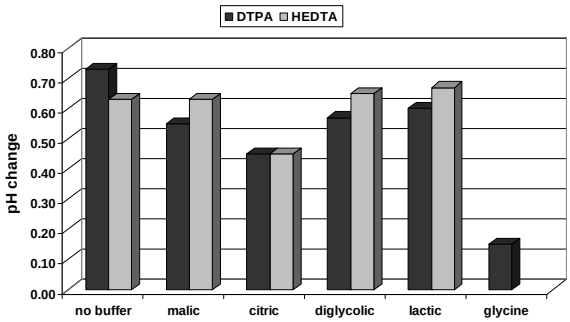

Fig. 7: The pH change for different buffers and complexing agents (pH change=$pH_{initial}$ – pH_{final}).

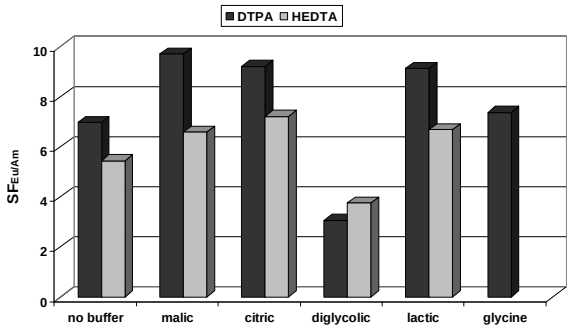

Fig. 8: The separation factors of ^{152}Eu over ^{241}Am for different buffers and complexing agents.

Between several tested buffers and selective complexants only two combinations gave satisfying results for both specified criteria (Table 2).

Table 2: The conditions for An stripping.

	Citric acid	Glycine
D_{Am}	0.10	0.47
D_{Eu}	1.14	3.31
$SF_{Eu/Am}$	11.4	7.0
Complexant	DTPA	DTPA
$pH_{initial}$	2.0	1.5

The last step, stripping of Ln, has not yet been tested; nevertheless we expect this step to be the less difficult one within the whole process. The efficient stripping should be achieved using 0.01 mol/L HNO_3. Scrubbing section has also been studied but the final conditions will be chosen shortly before a single centrifuge-contactor tests.

Conclusions

The batch tests of extraction and An-stripping section of the process for separation of An(III) from PUREX raffinate gave promising results. According to those results it is possible to co-extract An(III) together with Ln(III) and by using CDTA suppress the extraction of the problematic fission products (Pd, Zr). The final conformation of this process will be designing of a flow-sheet based on single centrifuge-contactor results and its implementation in a spiked counter-current test.

Acknowledgments

Financial support for this research was provided by the European Commission (project ACSEPT – No. 211267).

References

[1] G. Modolo, H. Asp, C. Schreinemachers, H. Vijgen, Solvent Extr. Ion Exch. 25 (2007), 703–721.

[2] X. Hérès, Ch. Sorel, M. Miguirditchian, B. Camès, C. Hill, I. Bisel, D. Espinoux, Global 2009, Paris, France, September 6-11, 2009.

[3] G. Modolo, H. Asp, H. Vijgen, R. Malmbeck, D. Magnusson, Ch. Sorel, Solvent Extr. Ion Exch. 26 (2008), 62–76.

Synthesis of Uranium-based Microspheres for Transmutation of Minor Actinides

H. Daniels, S. Neumeier, G. Modolo

Institut für Energieforschung, Sicherheitsforschung und Reaktortechnik (IEF-6),
Forschungszentrum Jülich GmbH, 52425 Jülich, Germany
Tel: +49(0)2461616282, Fax: +49(0)2461612450
Corresponding author: h.daniels@fz-juelich.de

Abstract: Utilisation of the internal gelation process is a promising perspective for the fabrication of advanced nuclear fuels containing minor actinides (MA). The formulation of appropriate precursor solutions for this process is an important step towards a working process as the chemistry of uranium-MA systems is quite complex. In this work, non-radioactive actinide surrogates were utilised for basic research on their influence on the system. The ceramics obtained through thermal treatment of the gels were characterised to optimise the calcination and sintering process.

Introduction

An alternative to the direct disposal of long-lived radionuclides is their separation from the original waste and subsequent transmutation. One promising concept after the partitioning step is embedding the minor actinides (MA: Am, Cm, Cf) in uranium-based nuclear fuel by an internal gelation process. This will allow the MAs to be destroyed by fast-neutron reactions in the upcoming generation-IV reactors.

The method for the internal gelation of uranium was developed by the KEMA laboratory in the 1960s and is based on the decomposition of hexa-methylene-tetra-amine (HMTA), after its protonation, to ammonia in heat. This causes a drastic pH increase, resulting in hydrolysis and condensation reactions. The reactions taking place are illustrated in equations (1) to (4):

$$[(CH_2)_6N_4] + H^+ \leftrightarrow [(CH_2)_6N_4H]^+ \quad (1)$$

$$[(CH_2)_6N_4H]^+ + 6\ H_2O + 3\ H^+ \rightarrow 4\ NH_4^+ + 6\ CH_2O \quad (2)$$

$$UO_2^{2+} + 2\ H_2O \leftrightarrow UO_2(OH)_2 + 2\ H^+ \quad (3)$$

$$UO_2(OH)_2 + H_2O \rightarrow UO_3 \cdot 2H_2O\downarrow \quad (4)$$

(1) *HMTA protonation,* (2) *HMTA decomposition,* (3) *Uranyl hydrolysis,* (4) *Uranyl condensation*

Several studies have been carried out on the whole subject and a common element for the fabrication of U(VI) gels is the need for a so-called acid-deficient uranyl-nitrate solution (ADUN) as precursor solution. This allows the use of a reduced quantity of HMTA due to the lower initial acidity. Moreover, a substoichiometric amount of nitrate improves the solubility of uranium and therefore allows higher concentrations. Understanding the influence of this step is crucial for the development of a working process. [1, 2, 3]

As the MAs, unlike uranium, are present in a trivalent oxidation state in the precursor solution, special attention has to be paid to their gelation behaviour, as well as to their distribution and structural influence in the gel. Therefore, in this work, Nd^{3+} was used as an MA surrogate to investigate the influence of such cations on the system. This is reasonable as the chemical properties of trivalent actinides and their corresponding lanthanides are very similar.

During the thermal treatment, phase transitions of the uranium matrix occur. After calcination at about 800 °C, uranium is present in the form of U_3O_8 which has a layered orthorhombic crystal structure [4]. Introducing quantitative amounts of trivalent actinides can have a certain impact on the mixed crystallographic structures whose characteristics at the molecular scale are to be investigated within this study.

Preparation of Acid-Deficient Uranyl-Nitrate

There are different ways of preparing ADUN. Amongst these are: dissolution of U_3O_8 in an understoichiometric amount of HNO_3, chemical removal of nitrate by a reducing agent like formic acid, and the extraction of HNO_3 from a uranyl-nitrate solution by amines [5].

After a series of preliminary tests, we decided to focus on extractive denitration with Primene JM-T (denoted in the following as Primene, a primary amine, M=269 g/mol, Figure 2) and this process was further investigated. Therefore, experiments concerning the appropriate molar ratio of Primene versus nitrate were undertaken: varying amounts of Primene were contacted with a uranyl-nitrate solution of which afterwards the corresponding pH and the ratio [Nitrate] / [Uranium] was determined. As seen in Figure 1, and as expected, with increasing amounts of Primene, the resulting nitrate-uranium ratio decreases after extraction in the aqueous solution while the pH increases. Taking the average of 0.7 moles nitrate extracted per mole Primene into account, a 1:1 extraction mechanism as shown in Figure 2 can be assumed. This leads to a simple method for estimating the required amount of Primene by assuming a linear coherence between the amount of Primene used and the amount of nitrate extracted.

It was found that with a pure 2.1-molar uranyl-nitrate solution, a denitration ratio of about 30 % can be achieved without forming precipitates. On the contrary, a typical internal-gelation stock solution (containing uranium, actinide surrogates and urea) starts to form precipitates at a ratio of more than 25 %. Therefore, the corresponding ratio of the denitrated stock solutions should be targeted to a value of not more than 20 %.

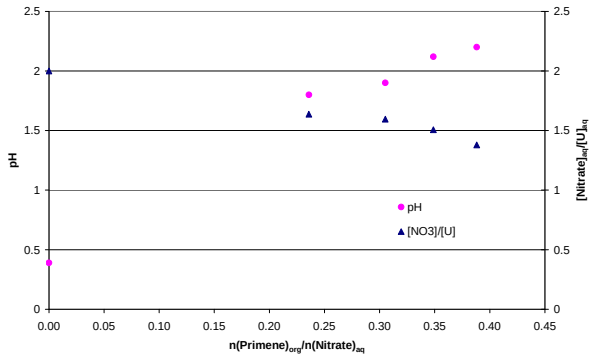

Fig 1: n(Primene) / n(Nitrate) ratio for extraction from a uranyl-nitrate solution in relation to resulting pH and [Nitrate] / [Uranium] ratio of the aqueous phase.

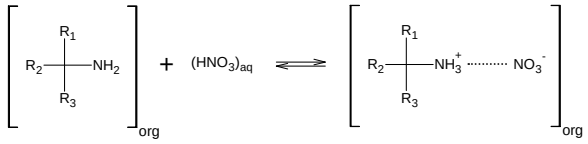

Fig. 2: Nitrate extraction with Primene.

Fabrication of Uranium-Neodymium Microspheres

An adapted internal gelation process as illustrated in Figure 3 was used to create uranium / neodymium microspheres [6]. A stock solution consisting of uranyl-nitrate, Nd-nitrate, urea and HMTA was created and dropped into hot silicone oil in which the gelation took place. As the spheres travelled from top to bottom in the gelation column, an increase in opacity was observed.

The obtained spheres were washed in petrol ether and ammonia solution and the metal losses in the washing solutions were measured via ICP-MS to evaluate the integrity of the gels. As all metal-concentrations in the washing solutions were in the range of 10^{-7} M to 10^{-6} M, this indicates not only complete gelation but already a certain leaching resistance.

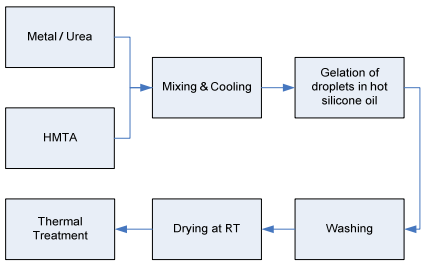

Fig. 3: Flow sheet for internal gelation process.

Afterwards, the microspheres were dried at room temperature before the thermal treatment took place. Drying at room temperature led predominantly to shrinkage of the microspheres without visible crack formation. Nevertheless, the usage of too less HMTA resulted in defects after drying, when no denitrated stock solution was used.

Calcination was carried out at 800 °C and SEM analysis was used as an initial indicator for the quality of the obtained product. After calcination, the SEM analysis showed that the spheres generally remained intact without visible phase segregation, but crack formation was present in dependence on the initial precursor solution formulation. An amount of 2.5 moles HMTA per mole metal caused cracks, while a decrease to 2.2 moles HMTA per mole metal led to an integer surface (Figure 4).

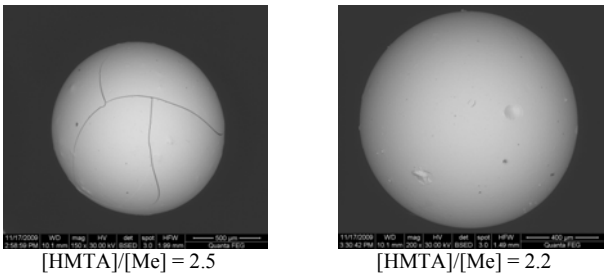

[HMTA]/[Me] = 2.5 [HMTA]/[Me] = 2.2

Fig. 4: SEM of calcinated U/Nd microspheres: 90% uranium & 10% neodymium; 800 °C.

Conclusion

This work demonstrates the general feasibility of an internal gelation process for creating uranium / neodymium microspheres with optional usage of acid-deficient uranyl-nitrate.

A method for extractive denitration with Primene of highly concentrated uranium solutions was evaluated. The experimental outcome led to a procedure allowing direct denitration of internal gelation stock solutions by extraction.

Fabrication of microspheres via an adapted internal gelation process with subsequent calcination of the gels was successfully carried out. Microspheres with an integer, crack-free surface were obtained when proper formulation and treatment of the stock solutions were applied.

Acknowledgements

Financial support for this research was provided by the European Commission (project ACSEPT – No. 211267).

References

[1] J. L. Collins, M. H. Lloyd and R. L. Fellows, Radiochim. Acta, 42 (1987) 121-134.
[2] R. D. Hunt and J. L. Collins, Radiochim. Acta, 92 (2004) 909-915.
[3] V. N. Vaidya, S. K. Mukerjee, J. K. Joshi, R. V. Kamat and D. D. Sood, J. Nucl. Mater., 148 (1987) 324 - 331.
[4] G. C. Allen and N. R. Holmes, J Nucl Mater., 223 (1995) 231-237.
[5] A. Deptula, C. Majani, ENEA (1986)
[6] R. Förthmann, A. Naoumidis, H. Nickel, W. Burck Forschungszentrum Jülich GmbH (1970).

Conditioning of Minor Actinides in Monazite-type Ceramics

C. Babelot, S. Neumeier, A. Bukaemskiy, G. Modolo, H. Schlenz, D. Bosbach

Institut für Energieforschun - Sicherheitsforschung und Reaktortechnik (IEF-6)
Forschungszentrum Jülich
Tel: +49(0)2461612752, Fax: +49(0)2461612450
Corresponding author: c.babelot@fz-juelich.de

Abstract: Monazite-type ceramics are promising candidates for the conditioning of minor actinides. Monazite ($LaPO_4$) was prepared by hydrothermal synthesis and its hydrated form ($LaPO_4{\cdot}0.5H_2O$) was synthesised by precipitation. The first characterisation results, structural and morphological combined with thermal behaviour and physical properties, are presented.

Introduction

In Germany, spent nuclear fuel and relatively small amounts of vitrified high level waste (from reprocessing in France and the UK) will be disposed in a deep geological formation. In principle, these waste forms seem to be suitable to accommodate the long-term safety of a waste repository system over extended periods of time. However, by using significantly more stable waste forms, the long-term safety of nuclear disposal could be significantly improved. Various ceramic waste forms seem to be promising materials in particular for tri- and tetravalent actinides, which dominate the long-term radiotoxicity [1; 2].

Here, we are studying lanthanide and actinide bearing monazite with respect to its stability under repository relevant conditions and in particular because of its stability against radiation damage [3]. *RE*PO_4 ceramics are named after their natural mineral analogue: monazite for *RE* = La to Gd (monoclinic structure) and xenotime for *RE* = Tb to Lu and Y (tetragonal structure).

The processes used to synthesise these samples were aqueous chemical routes such as hydrothermal synthesis and precipitation. Indeed, to avoid radioactive dust formation, synthesis routes like conventional solid state reaction are not advisable. Structural and morphological results applying XRD and SEM are presented here combined with thermal behaviour and physical properties.

Monazite and Rhabdophane

Wet-chemical methods were applied in this work for the preparation of monazite ($LaPO_4$) and rhabdophane ($LaPO_4{\cdot}0.5H_2O$). Monazite samples were prepared by hydrothermal synthesis (T=200°C). This fabrication process partly followed that described by Meyssamy [4]. Rhabdophane powders were synthesised by precipitation from lanthanum–citrate chelate solution (La–Cit) and phosphoric acid (at room temperature). This process was partially adapted from the route described by Boakye et al. [5].

In order to study the impact of calcination on these ceramics, the thermal behaviour of the dried powders was investigated from room temperature up to 1000°C by thermogravimetry (TG) coupled with differential scanning calorimetry analysis (DSC) in air atmosphere with a heating rate of 10 K/min. Fig. **1** shows the comparison of the TG-DSC measurements for monazite and rhabdophane (at pH=5 after washing). The mass loss of the monazite sample is about 4% while the one of the rhabdophane is about 10% after a thermal treatment up to 1000°C. This difference is partly caused by the residual crystal water contained in the rhabdophane structure.

For both powders a broad endothermic peak is observed between 100 and 200°C, which can be explained by the elimination of adsorbed gas and residual water. For the rhabdophane powder, an additional endothermic peak at ~270°C is observed which is linked to the elimination of the 0.5 mol of the crystal water.

The broad exothermic peak between 600 and 800°C belongs to the phase transformation from hexagonal to monoclinic (from rhabdophane to monazite) structure. Naturally, this peak does not appear on the monazite plot (magenta plot).

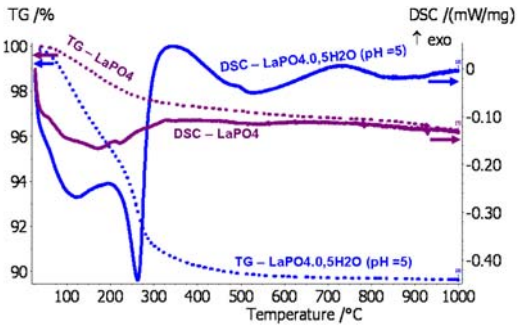

Fig. 1: TG-DSC measurements of monazite and rhabdophane (washed until pH=5) powders.

Fig. **2** shows the X-ray diffraction patterns of the dried monazite (first) and rhabdophane (second) powders.

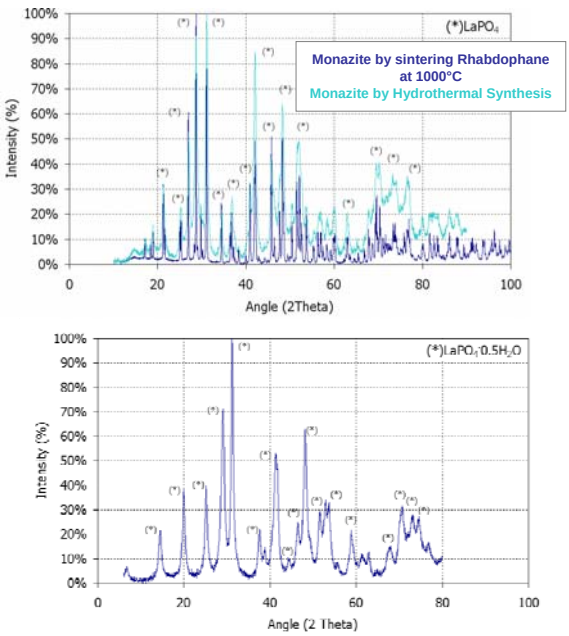

Fig. 2: XRD patterns of monazite obtained after hydrothermal synthesis and by calcination of rhabdophane (first). XRD of rhabdophane for comparison (second).

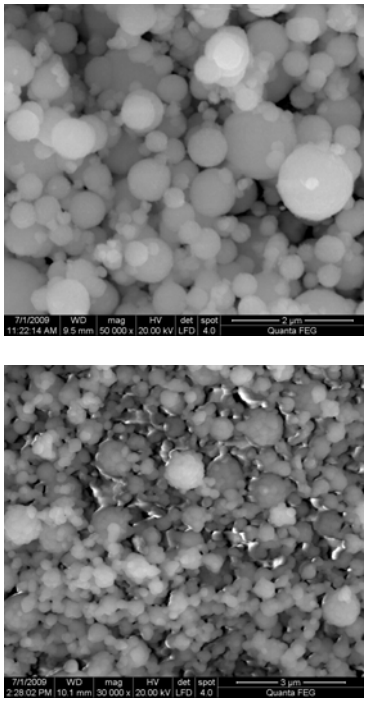

Fig. 3: SEM images of $LaPO_4 \cdot 0.5H_2O$ sample (first) and of calcined (1000°C) $LaPO_4 \cdot 0.5H_2O$ sample (second).

The XRD result of the monazite ($LaPO_4$) sample confirms that the phase is pure within the limits of the method. After calcination of the rhabdophane powder at 1000°C, XRD data show the similitude of the monazite (light blue) and the calcined rhabdophane (dark blue). The hexagonal to monoclinic phase transformation occurs. The FWHM (full width at half maximum) decreased for the 1000°C-calcined rhabdophane due to beginning of the material recrystallization (microstrain ε, crystallite size d). The diffractogram of rhabdophane powder also confirms the purity of this phase just after the precipitation.

The morphology of the powder was studied with scanning electron microscopy (SEM) as shown in Fig. **3**. The rhabdophane particles were round and their diameters is between 0.1 and 2 µm.

Since the phase transformation (hexagonal to monoclinic) takes an end around 850°C, the rhabdophane particles were heated up to 1000°C, where they consolidate together. This is the beginning of the sintering process. The comparison between the first and the second photo in Figure 3 shows significantly the beginning of the densification.

In this work, leaching tests are planed to be done on both powder and pellets. Indeed leaching tests on pellets is a standard method (e.g. Soxhlet method) and a study on pellet density is necessary.

The investigated powders were compacted by cold uniaxial pressing, applying pressures between 130 and 510 MPa. The pellets were made by powder synthesised by hydrothermal synthesis. The relative green density and the relative sintered density both depend on the applied pressure (see Fig. **4**). The results of the relative green density in relation to the logarithm of the pressure show that the values form a linear function. This is a typical behaviour for ceramic materials [6]. After the sintering at 1400°C [7], the relative sintered density of the pellets was determined by Archimedes method, i.e. by hydrostatic weighing in water (see second Figure). The value of the pressure related to the maximal density - optimal pressure - is between 250 and 400 MPa. The sintered density at this optimal pressure is above 98% of theoretical density.

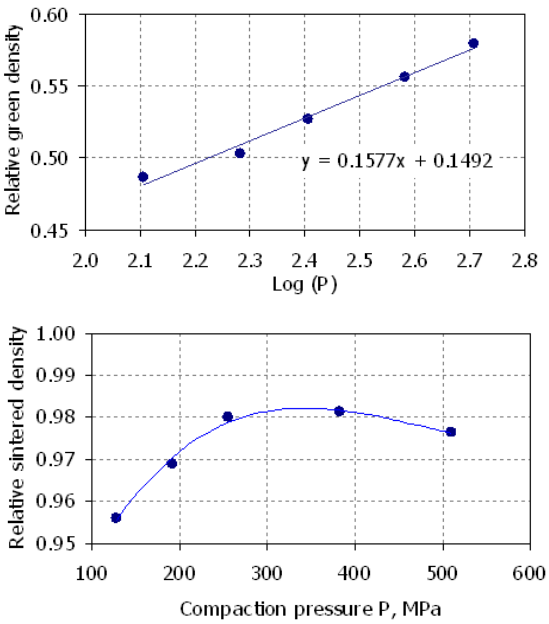

Fig. 4: Compressibility curve for monazite powders (first) and relative sintered density of monazite pellets, as a function of compaction pressure (second).

Conclusion and outlook

Monazite-type ceramics, as a promising candidate for the conditioning of minor actinides, were studied in this work. Monazite ($LaPO_4$) and Rhabdophane ($LaPO_4 \cdot 0.5H_2O$) powders were prepared by hydrothermal synthesis (T=200°C) and by precipitation (room temperature). The thermal analysis and XRD show that the monazite powders are already crystalline after synthesis and subsequent drying, whereas the Rhabdophane transforms at temperatures over 800°C to the monoclinic monazite structure. On the base of the synthesised monazite powder, pellets with a 98% of the theoretical density were prepared by cold pressing and sintering.

In order to simulate actinide integration into the lattice structure of the monazite-type matrix, lanthanide-doped monazite/xenotime matrices, $La_{(1-x)}Ln_xPO_4$ (Ln = Nd, Eu, Gd or Er, x = 0.10 to 1.00) have been synthesised, but have yet to be characterised. The full characterisation of the ceramic compounds is in progress and it is foreseen to study also the behaviour of immobilized actinides, such as americium and curium.

Primary focus of this work is the study of the thermodynamic properties of the solid matrices. Molecular level process understanding of ceramic waste form behaviour under repository conditions by using state-of-the-art spectroscopy (TRLFS) and microscopy technique (TEM) is planned. The corrosion behaviour of synthetic ceramics will be investigated. To this end, the ceramics will be subjected to leach tests under conditions of relevance for final repositories. The second essential parameter describing the stability of the host phases is the resistance to radiation. Radiation damage to the monazite type ceramics will be induced either by direct doping with radioactive nuclides or by means of ion bombardment.

Aknowledgements

This work is supported by the Ministerium für Innovation, Wissenschaft, Forschung und Technologie des Landes (MIWFT) Nordrhein-Westfalen; AZ: 323-005-0911-0129.

References

[1]. G. R. Lumpkin, Elements 2 (2006) 365-72.

[2]. P. Trocellier, Annales De Chimie-Science Des Materiaux 26 (2001) 113-30.

[3]. E. H. Oelkers and J. M. Montel, Elements 4 (2008) 113-16.

[4]. H. Meyssamy, K. Riwotzki, A. Kornowski, S. Naused, and M. Haase, Advanced Materials 11 (1999) 840.

[5]. E. E. Boakye, P. Mogilevsky, and R. S. Hay, Journal of the American Ceramic Society 88 (2005) 2740-46.

[6]. A. A. Bukaemskiy, D. Barrier, and G. Modolo, Journal of the European Ceramic Society 29 (2009) 1947-54.

[7]. D. Bregiroux, S. Lucas, E. Champion, F. Audubert, D. Bernache-Assollant, Journal of the European Ceramic Society 26 (2006) 279-287.

Radionuclide release from research reactor fuel

H. Curtius, G. Kaiser, E. Müller

Institut für Energieforschung – Sicherheitsforschung und Reaktortechnik (IEF-6),
Forschungszentrum Jülich
Corresponding author: h.curtius@fz-juelich.de

Abstract: In order to determine the corrosion behavior and the radionuclide release fractions of different irradiated research-reactor fuel-types in final repository relevant solutions investigations in a hot cell facility were performed. The dissolution of two dispersed research reactor fuel-types (UAl_x-Al and U_3Si_2-Al) was studied in $MgCl_2$-rich salt brine in the presence of iron-II-ions. Both fuel types corroded within the experimental time period of 3.5 years completely. In comparison, LWR spent fuel corroded only up to 0.01 %under comparable conditions after 2 years. After complete corrosion of the used research reactor fuel samples the inventories of Cs and Sr were detected in solution quantitatively. Solution concentrations of Am were lower than the solubility of $Am(OH)_3$ (s) and may be controlled by sorption processes. Pu concentrations may be controlled by Pu(VI), Pu (V) and Pu(IV) (hydr)oxides. Solution concentrations of U were within the range of the solubility limits of uranite. In comparison of both fuel samples the determined solubilities of U, Pu and Am were about one order of magnitude higher for the U_3Si_2-Al fuel sample. Here the formation of U/Si containing secondary phase components and their influence on radionuclide solubilities can not be ruled out.

Introduction

The final disposal of spent nuclear fuel in deep geological formations is considered as waste management option. In comparison to commercial spent fuel elements (UO_2 is the fuel) used in nuclear power plants, different spent research reactor fuel-types exist. At IEF-6 the work is focused on research reactor fuel. Two different fuel-types (a dispersed metallic UAl_x-type and the U_3Si_2-Al-type) are under investigation. One back-end option for these fuel-types is final disposal [1]. Possible repositories under consideration are salt and clay formations. Clay formations always contain clay pore waters. For salt formations the contact of spent fuel with an aquatic phase is a hypothetical scenario which is taken into account with respect to long-term safety analysis. These saline solutions will then start to corrode the steel canister and then the fuel cladding while producing large amounts of hydrogen. Also radiolysis of aqueous solutions is accompanied by the formation of redox agents [2]. In salt brines, H_2 molecules are the main reductants whereas radiolytic oxidants are dominated by oxo-halogenides [2].

In the presence of hydrogen overpressure the oxidative dissolution of LWR spent fuel, (consists of UO_2 as fuel cladded with Zircalloy), is decelerated. Only 0.01% of this fuel type corroded in a concentrated salt solution in the presence of container material (iron) in 2 years [3].

Under comparable conditions this paper describes for the first time the corrosion behaviour of two different irradiated dispersed research reactor fuel-types in a highly concentrated salt brine at 90 °C under static conditions in the presence of iron-II.

Experimental details

Static corrosion tests were performed under anoxic conditions in Ar-atmosphere in a hot cell facility at 90°C using glass autoclaves. Two different irradiated research reactor fuel types were used: a.) metallic UAl_x-fuel (fifa: 45%) and b.) U_3Si_2-fuel (fifa: 63%). Details with respect to the fuel dimension, fuel mass and radionuclide inventories are given in [4]. Solutions were sampled under Ar-atmosphere nine times per test and at test termination after 3.5 years. Gas sampling was performed nine times per test. More details and the analytical procedure are given in detail in [4].

Results and Discussion

The irradiated UAl_x-Al and U_3Si_2-Al fuel samples corroded completely within the 3.5 years of the experimental time period. Due to the corrosion processes secondary phases were formed. Hydrogen was produced due to the corrosion of the fuel cladding and due to radiolytic processes. The complete amounts of hydrogen were determined to be in the range of 0.11 mol. At test termination the measured pH-values were in the range of 5.0 (corrected value according to [5]).

In Figure 1 the radionuclide concentrations after complete corrosion of dispersed UAl_x-Al and U_3Si_2-Al fuels in $MgCl_2$-rich brine are summarized.

The amounts of Sr in solution represent the amount of the initial Sr inventories with respect to both fuel samples. The Sr release is considered to be the indicator of the progress of matrix dissolution, hence if the complete Sr inventory is in solution the fuel did dissolve completely. This is based on the assumption that the Sr inventory is contained in the fuel matrix, where it is distributed homogeneously. The corrosion rates were determined to be $7.69 \cdot 10^{-3}$ g/m^{2}d for the UAl_x-Al fuel sample and $4.24 \cdot 10^{-2}$ g/m^{2}d for U_3Si_2-Al fuel sample.

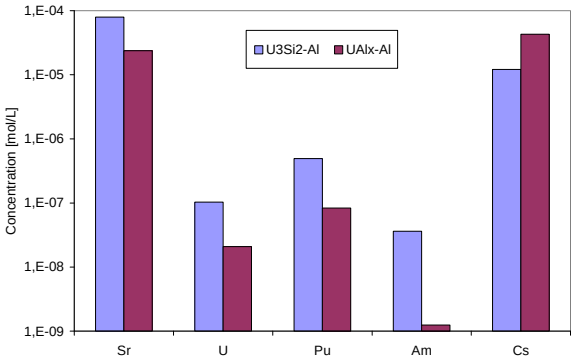

Fig. 1: Final solution concentrations of radionuclides after corrosion of the dispersed UAl_x-Al and U_3Si_2-Al fuels in $MgCl_2$-rich brine under initial Ar atmosphere

The final U concentrations for both fuel types were determined to be 10^{-8} to 10^{-7} M (pH 5). The solubility of $U(OH)_4$ (am) under comparable conditions in a 5.6 M NaCl solution [6] was determined to be in the range of 10^{-9} to 10^{-7} M. Therefore the assumption can be drawn that the component $U(OH)_4$ (am) is the main U containing phase present. The solubilities of hexavalent U components like metaschoepite (UO_3 $2H_2O$(cr)) or Na-diuranate ($NaUO_2O(OH)$(cr) are significant higher and do not agree with the measured U solubilities in these experiments, hence the presence of these phases may be ruled out. Nevertheless in the case of the U_3Si_2-Al-fuel different U components can be formed. It was observed during corrosion of UO_2 in spent fuel under reducing conditions that coffinite ($USiO_2$ 2 H_2O) may form [7]. Also coffinite may not be the only phase replacing uranite and spent fuel under these conditions. Recently an unnamed uranium silicate with a stoichiometry close to U_3SiO_8 has been reported [6]. In conclusion that means that in case of the U_3Si_2-fuel corrosion under reducing conditions the presence of these alteration products may not be ignored.

The measured Pu concentrations were in the range of 10^{-7} to 10^{-6} M (pH=5). As observed in other studies these concentrations might describe a mixture of Pu-IV, Pu-V and Pu-VI hydro (oxy) species [6].

The determined final Am concentrations for the UAl_x-Al fuel sample was about 10^{-9} M and about 10^{-8} M for the U_3Si_2-Al sample. This values are lower as the solubility of amorphous Am $(OH)_3$(s). Runde [8] measured that amorphous Am $(OH)_3$(s) is expected as solubility controlling phase in high concentrated salt solutions and the solubility of amorphous Am $(OH)_3$(s) was determined to be about 10^{-7} M. Processes which may retain Am are coprecipitation with secondary U phases and sorption on iron corrosion products.

In general the concentrations for the radionuclides U, Pu and Am were determined to be about one order of magnitude higher for the used U_3Si_2-Al fuel sample in comparison to the UAl_x-Al fuel sample. As discussed above the formation of U and Si containing solids as corrosion products can not be excluded. These U/Si containing solids may influence the radionuclide concentrations through their solubilities and their retention capacities.

Conclusion and outlook

Results of this work confirm the instantaneously corrosion of the research reactor UAl_x-Al and U_3Si_2-Al fuel types within the test period of 3.5 years in the presence of iron-II and in the $MgCl_2$-rich brine. The complete corrosion of the fuel samples was confirmed by the final Sr concentration in solution which represented the initial complete Sr inventory in the fuel. Especially the solution concentration of the trivalent actinide Am is orders of magnitude lower than the solubility of pure Am(III) hydroxide phase and appear to be controlled by coprecipitation phenomena. Comparing the behaviour of both fuel-types an influence of Si was observed. In the presence of Si the solubilities of U, Pu and Am are one order of magnitude higher. This can be due to the formation of U/Si containing solids.

Further research is recommended to determine the influence of Si in detail. The synthesis of coffinite, the determination of its solubility and the formation of solid solutions with trivalent actinides are aspired.

References

[1] Thamm, G.: Disposal of irradiated fuel elements from German research reactors – Status and Outlook; Trans. Int. Conf. Research Reactor Fuel Management (RRFM 1999), Bruges, Belgium, 159 (1999).

[2] Metz, V., Loida, A., Bohnert, E., Schild, D., Dardenne, K., Effects of hydrogen and bromide on the corrosion of spent nuclear fuel and γ-irradiated UO_2(s) in NaCl brine, Radiochim. Acta **96**, 637 (2008).

[3] Loida, A., Grambow, B., Geckeis, H., Anoxic corrosion of various high burnup spent fuel samples, Journal of Nuclear Materials, **238**, 11 (1996).

[4] Curtius, H., Kaiser, G., Paprigas, Z., Ufer, K., Müller, E., Enge, R., Brücher, H., Untersuchungen zum Verhalten von Forschungsreaktorbrennelementen in den Wirtsgesteinsformationswässern möglicher Endläger, Berichte des Forschungszentrums Jülich, 4237, ISSN 0944-2952. (2006).

[5] Grambow, B., Müller, R., Chemistry of corrosion in high saline brines, Mater. Res. Soc. Symp. Proc. **176**, 229 (1990).

[6] Loida, A., Grambow, B., Geckeis, H., Dressler, P., Process controlling radionuclide release from spent fuel, Mat. Res. Soc. Symp. Proc. **353**, 577 (1995).

[7] Janeczek, J., Ewing, R.C., Coffinitization – A Mechanism for the Alteration of UO2 under Reducing Conditions, Mat. Res. Soc. Symp. Proc. **257**, 497 (1992).

[8] Runde, W., Zum chemischenVerhalten von drei- und fünfwertigen Americium in salinen NaCl-Lösungen" Dissertation, Technische Universität München (1993).

Separation and enrichment of secondary phases of research reactor fuel elements and identification by SEM-EDX

M. Klinkenberg, H. Curtius

Institut für Energieforschung – Sicherheitsforschung und Reaktortechnik (IEF-6), Forschungszentrum Jülich
Corresponding author: m.klinkenberg@fz-juelich.de

Abstract: The corrosion products of research reactor fuel elements of the UAl_x-Al-type in $MgCl_2$-rich brine were investigated. This study contributes to the long-term safety analysis of direct disposed research reactor fuel elements in deep geological repositories (salt formations) because secondary phases may serve as a barrier against radionuclide migration. For a better identification of the secondary phases a sample treatment is necessary. Therefore, a grain size fractionation was carried out and different solvents were used to enrich single secondary phases. A chemical and mineralogical characterisation of the secondary phases was accomplished.

Introduction

In contrast to UO_2 fuel elements which are used in commercial nuclear power plants, research reactor fuel elements are composed of metallic UAl_x-Al or U_3Si_2-Al. Corrosion experiments with non-irradiated dispersed metallic UAl_x-Al-fuel in highly-concentrated $MgCl_2$-salt brine were performed [1]. The fuel elements corroded within a few months. Previous studies showed that the radionuclides were rapidly mobilized during the corrosion process, but then trapped by secondary phases [2].

In order to improve the identification and quantification of these secondary phases, an enrichment of single phases is necessary. The identification by XRD is difficult due to the high amount of amorphous phases and overlapping peaks of phases like bischofite ($MgCl_2 \cdot 6\ H_2O$)) which derive from the brine, as well as a high water content of the samples. The main topic of this study is the morphological and chemical characterisation of the obtained grain size fractions by SEM/EDS.

Experimental details

Sample preparation and enrichment of secondary phases – UAl_x-Al fuel element plates corroded under Ar-atmosphere in 400 mL $MgCl_2$-rich salt-brine (Tab. 1) at 90 °C. Additionally 10 g $Fe(II)Cl_2 \cdot 4\ H_2O$ was added to simulate the presence of Fe due to the corrosion of the container.

Table 1: Chemical composition of the brine [3].

Ca [mol/L]	Cl [mol/L]	K [mol/L]	Mg [mol/L]	Na [mol/L]	SO_4 [mol/L]	pH corr.
0.2690	9.8456	0.0190	4.6014	0.0706	0.0005	6.03

For the enrichment of single phases of the corrosion products a method was used which is successfully applied in soil science and clay mineralogy [4]. The grain size fractions > 63 µm, 2-63 µm, and < 2 µm of the samples were obtained by sieving and the use of Atterberg cylinders.

Different solvents (acetone, iso-propanol and water) were used in order to dissolve interfering phases e.g. bischofite or other salts remaining from the brine. The obtained substances were characterized by ICP-OES, LSC, alpha-spectrometry, and SEM-EDS.

Chemical analysis – The chemical composition of the untreated sample (liquid and solid phase) was determined. For the determination of Al and Fe, ICP-OES was used. The U content was determined from activity measurements by LSC and alpha-spectrometry.

Scanning electron microscopy (SEM) – For the characterisation of the solid corrosion products SEM combined with EDS (energy dispersive x-ray spectroscopy) was used. The environmental SEM Quanta 200 F manufactured by FEI and equipped with the EDX-system Genesis (EDAX) was used for the investigations. Samples were prepared as powders/grains on carbon tabs and measured in low-vacuum mode.

Results

Chemical composition – The results of the Al determination (Tab. 2) show that for both samples only a minor amount of Al is dissolved in the aqueous solution (1 - 2 wt.-%). Hence, Al is determined to be in the solid state.

Table 2: Al and Fe contents (ICP-OES) and U contents (LSC, alpha-spectroscopy) for the solid and aqueous solution (pH 5.3 after corrosion) phases of the corrosion products.

	Al		Fe		U	
	[g]	[wt.%]	[g]	[wt.%]	[g]	[wt.%]
A6 2008 (UAl_x-Al, brine 2, Fe)						
Reference	**1.88**	**100**	**2.80**	**100**	**0.12**	**100**
Liquid	0.02	1	1.48	53	0.001	1
Solid	1.63	87	1.03	37	0.118	98
Liquid + Solid	**1.65**	**88**	**2.51**	**90**	**0.119**	**99**
AA6 2008 (UAl_x-Al, brine 2, Fe)						
Reference	**1.88**	**100**	**2.80**	**100**	**0.12**	**100**
Liquid	0.03	2	1.56	56	0.006	5
Solid	1.52	81	0.88	31	0.121	101
Liquid + Solid	**1.55**	**83**	**2.44**	**87**	**0.127**	**106**

About half of the iron (53 - 56 wt.-%) is dissolved in the liquid phase. 31-37 wt.-% is included in the solid phase (Tab. 2).

For U only a minor amount is dissolved in the liquid phase (1 - 5 wt.-%). The measurements of the U content reveal that U remains in the solid phase, but not in the aqueous solution.

Characterisation by SEM/EDS – An overview of typical crystalline phases and their morphologies, which were observed for secondary phases in the obtained fractions by SEM shows Fig. 1.

a) Sand rose structure consisting of thin platy crystals. These crystals are composed of Al, Mg, O, and Cl (sample A6 2008 iso-propanol > 63 µm). The morphology and the chemical composition are typical for LDHs (layered double hydroxide).

b) Cubic crystals consisting of Al, Cl, and O (sample A6 2008 iso-propanol < 2 µm). According to the morphology and chemical composition this phase is identified as lesukite ($Al_2(OH)_5Cl{\cdot}2H_2O$).

c) Aggregate of aluminium oxides/hydroxides consisting of Al and O (sample A6 2008 H_2O > 63µm).

d) The bright area of the large aggregate (150 µm) consists of U associated with Al (uncorroded fuel) and is surrounded by secondary phases, mostly Al-oxides/hydroxides (A6 2008 H_2O > 63µm).

e) Platy crystals of a Fe-phases consisting of Fe, O, and Cl (sample AA6 2008 iso-propanol > 63 µm).

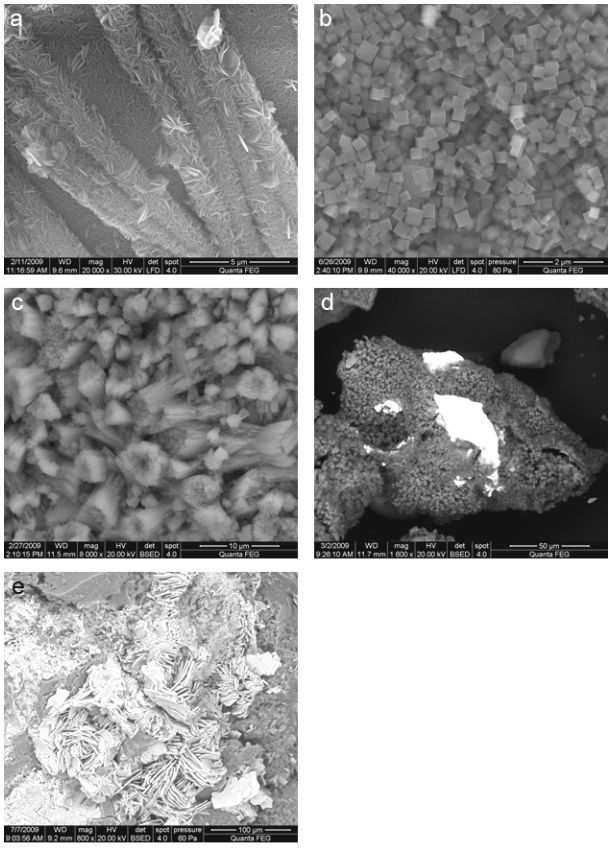

Fig. 1: **a)** LDH, A6 2008 iso-prop. > 63 µm
b) Lesukite, A6 2008 iso-prop. < 2 µm
c) Al-oxide/hydroxide, A6 2008 H_2O > 63µm
d) UAl_X (white), A6 2008 H_2O > 63µm
e) Fe-phases, AA6 2008 iso-prop. > 63 µm.

For the acetone treated samples a high content of bischofite deriving from the brine was observed. For the iso-propanol treated samples the following minerals could be identified: LDH, lesukite, Fe-phases, U associated with Al (uncorroded fuel) in coarser aggregates and Al-oxides/hydroxides. An enrichment of iron-minerals could be observed in the 2-63 µm fraction. Lesukite is enriched in the < 2 µm fraction. For the water treated samples an enrichment of Al-oxides/hydroxides, particularly in the < 2 µm fraction, could be observed. Only traces of LDH could also be found. Lesukite is completely dissolved by the water. Furthermore, small amounts of Fe-phases and uncorroded fuel occur.

An EDS-analysis of the fine fractions of the differently treated samples was performed. Several areas of different sites of the samples were measured, quantified, and mean values were calculated for the element contents. The results show that the highest Mg and Cl concentrations could be found for the acetone treated sample. Salts like bischofite deriving from the brine were not dissolved. The iso-propanol treated sample shows lower concentrations of Mg and Cl. Accordingly, the Al and O content is higher. Furthermore, Fe is enriched. The water treated samples show the lowest amounts of Mg and Cl and accordingly the highest concentrations of Al and O. Due to the highest solubility of water, lesukite was dissolved completely. These results confirm the observations made by SEM.

Conclusions

Due to the sample treatment various crystalline phases could be enriched successfully, which lead to a better identification of the secondary phases. From the results of the chemical investigation of the samples can be concluded, that Al and U are dissolved and reprecipitated. Hence, they are only present in the solid. The solid-phase characterisation by SEM/EDS suggests that the following crystalline secondary phases are identified: Mg-LDH, lesukite, Al-oxide/hydroxide and, Fe-phases. A high amount of amorphous phases (approximately 50 wt.-%) is contained in the samples as well. It is assumed that U is also associated to these amorphous phases. To clarify the binding mechanisms of U, a characterisation and quantification of the amorphous phases will follow in further investigations.

References

[1]. Brücher, H., Curtius, H., Fachinger, J., Kaiser, G., Mazeina, L., Nau, K.: Untersuchungen zur Radionuklidfreisetzung und zum Korrosionsverhalten von bestrahltem Kernbrennstoff aus Forschungsreaktoren unter Endlagerbedingungen, Report Forschungszentrum Jülich, Jül-4104, ISSN 0944-2952 (2002).

[2]. Mazeina, L., Curtius, H., Fachinger, J., Odoj, R.: Characterisation of secondary products of uranium-aluminium material test reactor fuel element corrosion in repository-relevant brine, J. Nucl. Mater. 323, 1 (2003).

[3]. B. Kienzler, A. Loida, (Hrsg.), Endlagerrelevante Eigenschaften von hochradioaktiven Abfallprodukten – Charakterisierung und Bewertung – Empfehlungen des Arbeitskreises HAW-Produkte; Wissenschaftliche Berichte FZKA 6651, Institut für Nukleare Entsorgungstechnik, Forschungszentrum Karlsruhe, (2001).
[4]. Hiltmann, W. & Stribrny, B.: Tonmineralogie und Bodenphysik. Handbuch zur Erkundung des Untergrundes von Deponien und Altlasten, Band 5. BGR, Bundesanstalt für Geowissenschaften und Rohstoffe. ISBN 3-540-59465-5 Springer-Verlag (1998).